Atmos. Chem. Phys. Discuss., 14, 1861–1917, 2014
www.atmos-chem-phys-discuss.net/14/1861/2014/
doi:10.5194/acpd-14-1861-2014

Atmospheric Chemistry and Physics
Open Access
Discussions

Critical assessment of meteorological conditions and airflow connectivity during HCCT-2010

A. Tilgner[1], L. Schöne[1], P. Bräuer[1], D. van Pinxteren[1], E. Hoffmann[1], G. Spindler[1], S. Mertes[1], W. Birmili[1], R. Otto[1], M. Merkel[1], K. Weinhold[1], A. Wiedensohler[1], H. Deneke[1], W. Haunold[2], A. Engel[2], A. Wéber[2], and H. Herrmann[1]

[1]Leibniz Institute for Tropospheric Research (TROPOS), Leipzig, Germany
[2]Institute for Atmospheric and Environmental Sciences (IAU), Goethe University Frankfurt, Frankfurt, Germany

Received: 11 December 2013 – Accepted: 18 December 2013 – Published: 21 January 2014

Correspondence to: H. Herrmann (herrmann@tropos.de)

Published by Copernicus Publications on behalf of the European Geosciences Union.

Abstract

This study presents a comprehensive and critical assessment of the meteorological conditions and atmospheric flow during the Lagrangian-type "Hill Cap Cloud Thuringia 2010" experiment (HCCT-2010). HCCT-2010 was performed in September and October 2010 at Mt. Schmücke in the Thuringian forest, Germany, applying three measurements sites (upwind, in-cloud, downwind) to study physical and chemical aerosol-cloud-interactions. A Lagrangian-type hill cap cloud experiment requires suitable cloud and particularly connected airflow conditions, i.e. representative air masses at the different measurement sites. Therefore, the present study aimed at the identification of time periods during the 6-weeks duration of the campaign, where such conditions were fulfilled and which can be used in further data examinations.

The following topics were studied in detail: (i) the general synoptic weather situations including the mesoscale flow conditions by means of a classification of advected air masses and calculation of non-dimensional flow parameters (e.g. Froude number), (ii) local meteorological conditions, including synoptic front passages, the presence of orographic or frontal cloudiness, cloud base heights and vertical stratification, and (iii) local flow conditions by means of statistical analyses using the quasi-inert trace gas ozone and selected size bins of particle number size distributions as well as SF_6 tracer experiments in the campaign area. A comprehensive analyses using statistical measures such as the COD (Coefficient Of Divergence) and cross-correlation have been carried out for the first time in the context of a Lagrangian-type hill cap cloud experiment. Suitable criteria for the aimed statistical analyses were thus developed and applied in the present study to characterise the local flow connectivity in detail.

The comprehensive examination resulted in a total of 14 so-called "Full Cloud Events" (FCE), which are shown to conform to the Lagrange-type experimental philosophy of HCCT-2010. In addition, 15 so-called "Non-Cloud Events" (NCEs) could be established, which can be used as reference cases as they provide similarly suitable flow conditions but no cloud at the summit site. Orographic cloudiness was identified

for approx. one third of the FCE periods, while about two thirds were associated to synoptic fronts. The statistical flow analyses indicate the existence of a strong link between the sites during the events, particularly under constant south-westerly flow conditions, high wind speeds and slightly stable stratification. The COD analyses using continuously measured concentrations of ozone and the 49 nm diameter particle bin revealed particularly for COD values below 0.1 very consistent time series, i.e. closely linked air masses between the different sites. The cross-correlation analysis revealed under connected flow conditions typical overflow times of about 15 to 30 min between the two valley sites. Additionally, the performed SF_6 tracer experiments during the campaign clearly demonstrate that under appropriate meteorological conditions a Lagrangian-type approach is valid and that the connected flow validation procedure developed in this work is suitable for identifying such conditions. Finally, an overall evaluation of the identified FCEs is presented, which provides the basis for subsequent investigations of the measured chemical and physical data during HCCT-2010.

1 Introduction

Clouds occupy on average approximately 15 % of the volume of the lower troposphere (Pruppacher and Jaenicke, 1995) and they play a crucial role for various physical and chemical processes in the troposphere (Heintzenberg and Charlson, 2009; Möller, 2010; Ravishankara, 1997). Thus, physical and chemical cloud processes clearly impact large-scale environmental change issues such as climate change and its societal implications (IPCC 2013). Due to the highly variable spatial and temporal occurrence as well as the altitude of clouds, investigations of physical and chemical interactions between gases, aerosol particles and cloud droplets are quite challenging and much less understood than pure gas phase processes. Several hill cap cloud experiments conducted in the past (at Kleiner Feldberg, Germany, in 1990 (Wobrock et al., 1994), at Great Dun Fell, UK, in 1993 and 1995 (Bower et al., 1999; Choularton et al., 1997), at Tenerife, Spain, in 1997 (Bower et al., 2000) and at Mt. Schmücke, Germany, in 2001

Discussion Paper | Discussion Paper | Discussion Paper | Discussion Paper |

ACPD

14, 1861–1917, 2014

Critical assessment of meteorological conditions and airflow connectivity

A. Tilgner et al.

and 2002 (Herrmann et al., 2005)) have shown that ground-based Lagrangian-type experiments, where an orographic cloud is used as a natural flow-through reactor, may be a useful concept to study cloud processes in detail. Ground-based cloud experiments offer the opportunity to characterise the gas phase, the aerosol particle phase, and the cloud droplet phase in much experimental detail before, during and after the cloud processing, thus enabling an advanced understanding of the chemical cloud effects and interactions. However, the use and quality of such Lagrangian-type hill cap cloud field campaigns strongly depends on the meteorological conditions and their correspondence to the connected flow and cloud passage concept. Therefore, a critical evaluation of meteorological conditions and flow connectivity conditions is strictly required before entering further investigations of the measured datasets (see Tilgner et al., 2005; Heinold et al., 2005).

In general, hill cap cloud experiments make use of the effect that air parcels can be forced to traverse a hill or a mountain ridge and that – under favourable conditions – the terrain-induced lifting cools down the air parcel so that an orographic cloud is formed near the mountain ridge. Under those "natural flow-through reactor" conditions, the cloud-induced changes to the budget of particle and gas phase compounds can be characterised by ground based field measurements conducted upwind, in-cloud, and downwind of the mountain ridge.

The connectivity of atmospheric flow across a mid-level mountain ridge can be evaluated on the basis of non-dimensional parameters like the Froude and Richardson numbers (see Heinold et al., 2005 and references therein). These parameters can be derived from the horizontal wind field as well as vertical stratification. An essential question is whether the incoming air parcel contains enough kinetic energy (wind speed) to ascent and pass over the mountain ridge under the present vertical thermal conditions. Thus, vertical stratification and wind shear come into play as well. In reality, the evaluation of flow connectivity can be complicated by non-homogeneous terrain, such as a variable crest line and changeable surface roughness. Therefore, other local

ACPD
14, 1861–1917, 2014

parameters also need to be used to assess the likelihood of an air parcel passing over a mountain ridge.

Besides the characterisation of the mesoscale overflow conditions with non-dimensional parameters, continuously measured tracer species can be used to ascertain the movement of an air parcel across the mountain ridge. Tracer species include, for example, relatively inert gas phase species, such as ozone (O_3), and selected size ranges of atmospheric aerosol particles that are not expected to be modified by a cloud passage, such as interstitial particles of a certain size. Another appropriate method to validate the flow connectivity are tracer experiments, which are performed only occasionally during the measurement campaigns (see Heinold et al., 2005 and references therein). Furthermore, the idea of equivalent and thus comparable air masses at all sites comprises also that the measurement periods are not affected by air mass changes (front passages) and precipitation throughout the measurement periods. Thus, besides the overflow characterisation, the synoptic and local meteorological conditions need to be assessed as well to finally evaluate the overall suitability of the present conditions for further investigations of the cloud passage experiment data.

The present work is aimed at the critical assessment of meteorological conditions and flow connectivity during the Hill Cap Cloud Thuringia (HCCT-2010) in order to provide evaluated periods with both adequate meteorological conditions and flow connectivity. HCCT-2010 was conducted in September and October 2010 at the Mt. Schmücke (937 m a.m.s.l.), which is part of the mountain ridge of the Thuringian Forest (Germany). The location was already used for the previous hill cap cloud campaigns FEBUKO (Field Investigations of Budgets and Conversions of Particle Phase Organics in Tropospheric Cloud Processes; see Herrmann et al., 2005 for further details), studying the meteorological conditions and airflow characteristics extensively (Tilgner et al., 2005; Heinold et al., 2005). During FEBUKO, model calculations and tracer experiments showed that the flow between the measurement sites was reasonably well-connected during many cloud events.

ACPD
14, 1861–1917, 2014

In preparation of the new field experiment HCCT-2010, we re-evaluated the former study and more recent meteorological data (2004–2008), finding a maximum probability for hill cap clouds to occur in the area during September and October. This run-up analysis showed, for example, that on 5 yr average, approximately 10 cloud events occurred per month in September and October, respectively, under suitable wind conditions (south-western wind direction). Therefore, it was decided to conduct HCCT-2010 during September and October 2010 due to the highest probability of the occurrence of warm orographic clouds in connection with south-westerly flow traversing the mountain range in perpendicular fashion.

In analogy to the former works at Mt. Schmücke (see Tilgner et al., 2005; Heinold et al., 2005), the present work examines the synoptic conditions, flow connectivity and other meteorological issues important for the experimental concept of the hill cap cloud experiment HCCT-2010. In a first step, the mesoscale conditions were evaluated with particular emphasis on the incident flow conditions and the properties of the air masses advected into the HCCT-2010 study area. In the following, the properties of local airflow were analysed in detail. In particular, the connectivity of atmospheric flow across the mountain ridge was assessed by meteorological, aerosol and gas phase parameters measured upwind, on top, and downwind of the mountain ridge. The entire measurement period was analysed using statistical measures with respect to the prevalence of the same air mass at all sites, irrespective of wind direction and the presence or non-presence of a cloud. Classification criteria are developed concerning two main issues: (i) whether the airflow was likely to be connected between the three observation sites across the mountain ridge and (ii) whether a hill cap cloud was present and likely to have influenced the air parcel travelling across the ridge. All selected reference periods of HCCT-2010 are further evaluated with respect to the question of flow connectivity and cloud conditions. Non-dimensional flow parameters such as the Froude number (Fr) are used to characterise the regional flow regime in mountainous terrain. For specific periods, the airflow is verified by dedicated tracer experiments using the inert gas SF_6. Moreover, the locally measured meteorological and microphysical data,

ACPD
14, 1861–1917, 2014

rawinsonde observations, satellite pictures, ceilometer data and calculated backward trajectories were used to investigate the selected event periods with respect to the separation of orographic and non-orographic clouds, the detection of frontal processes, the air mass advection and the cloud conditions. Finally, an overall evaluation of the obtained meteorological and connected flow investigation results is made in order to sufficient periods so-called FCEs and NCEs (full cloud events (FCEs)/non-cloud events (NCEs)) for the aimed subsequent investigations The aimed FCEs should be periods, where all predefined connected flow and cloud criteria for a suitable Lagrangian-type experiment are fulfilled (see Sect. 3.2 for details). On the other hand, the aimed NCEs should be periods with connected flow conditions but no cloud present at any measurement site.

2 Methods and implementation

2.1 Measurement site description

The hill cap cloud experiment HCCT-2010 was conducted at Mt. Schmücke in Thuringia, Germany, in September and October 2010. The summit of Mt. Schmücke belongs to the about 60 km long mid-level mountain chain of the Thuringian Forest, running northwest to southeast without any major gaps. Based on the experience of the former FEBUKO experiment (see Heinold et al., 2005), three ground-based measurement sites were established during HCCT-2010: Goldlauter (GL, nominal upwind site), Mt. Schmücke (SM, summit site), and Gehlberg (GB, nominal downwind site) (see Fig. 1). The upwind site Goldlauter (10°45′20″ E, 50°38′25″ N, 605 m a.m.s.l.) served as the site to characterise air parcels approaching to the experimental site under south-western flow conditions. The measurement site Mt. Schmücke (10°46′15″ E, 50°39′19″ N, 937 m a.m.s.l.), where the German Weather Service (Deutscher Wetterdienst, DWD) and the Federal Environmental Office (Umweltbundesamt, UBA) operate a research station, is located near the mountain ridge. Mt. Schmücke it-

ACPD
14, 1861–1917, 2014

self is in the vicinity of the highest peak of the Thuringian Forest (982 m a.m.s.l.). The summit site Mt. Schmücke served as the prime site to analyse physical and chemical aerosol and cloud droplet parameters. Lastly, the downwind site Gehlberg (10°47′32″ E, 50°40′21″ N, 732 m a.m.s.l.) served as the site to characterise air masses descending the downwind slope of Thuringian Forest mountain ridge under appropriate south-western (SW) flow conditions.

The offline sampling, i.e. experimental measurements with all instruments not running continuously, have been performed only under specific suitable conditions. Based on the experience of the former FEBUKO experiment (see Herrmann et al., 2005), the following six criteria have been used to perform offline sampling during HCCT in the context of a Lagrangian-type hill cap cloud experiment: (i) Liquid Water Content (LWC) of the summit site cloud above 0.1 $g m^{-3}$ (ii) wind direction from the south-west (200–250° sector) (iii) wind speed at Mt. Schmücke of at least 2 $m s^{-1}$ and not exceeding 12 $m s^{-1}$ (vi) no fog at the 2 valley sites (v) no precipitation at any site and (vi) air temperature above 0 °C. Further details on, why this required condition criteria were used, are outlined in Herrmann et al. (2005).

2.2 Characterisation of the local flow connectivity using Coefficient of Divergence (COD) of particles in the Aitken (49 nm) and accumulation mode (217 nm) range

Particle number size distributions were recorded continuously during HCCT-2010 at all three sites using four identical Scanning Mobility Particle Sizers (SMPS). Selected particle bins are used in the present study for characterisation of the local flow connectivity. Details on the performed SMPS measurements are given in the Electronic Supplement (ESM).

In order to investigate spatial variation of selected aerosol size bins between two measurement sites and thus to characterise the degree of similarity between particle data, the coefficient of divergence (COD, sometimes also abbreviated as CD) has been used as a statistical measure. The COD has been used in several studies (see e.g.,

ACPD
14, 1861–1917, 2014

Wongphatarakul et al., 1998; Pinto et al., 2004; Krudysz et al., 2008; Ott et al., 2008; Wang et al., 2011) to determine the relative spatial variability of measured particle mass and component concentrations among different sampling sites. Consequently, the COD can also be used to investigate the airflow over the mountain range by characterising the temporal similarities between measured particle data at the different HCCT-2010 sites. The COD is defined as

$$\mathrm{COD}_{a,b} = \sqrt{\frac{1}{n}\sum_{i=1}^{n}\left(\frac{x_{i,a}-x_{i,b}}{x_{i,a}-x_{i,b}}\right)^2} \tag{1}$$

where $x_{i,a}$ and $x_{i,b}$ represent, e.g., the ith aerosol number concentration measured at the site a and b, respectively. In Eq. (1), n represents the total number of data points considered in the calculation. In case that the obtained concentrations at the two sampling sites are very similar, the COD approaches zero. In contrast, the COD approaches unity in case of diverging concentration profiles. It should be noted that the COD represents a measure to compare two sites only and never all three stations at once. Therefore, for an overall comparison of the three HCCT-2010 sites, the COD of each site combination needs to be calculated and all three COD values have to be below a threshold to indicate similarity between particle data and finally connected flow conditions between the three measurement sites.

For the characterisation of the uniformity between aerosol data sets, the US EPA (US EPA, 2004) proposed COD criterions, which indicate both homogeneity and heterogeneity of the datasets. CODs larger than 0.2 indicate heterogeneity and values below 0.1 indicate homogeneity. This criterion is in agreement with findings of other studies reported in the literature, which used a COD of 0.2 as reference value. For the characterisation of the overflow, this means that lower CODs indicate good flow connectivity conditions and larger CODs indicate flow conditions, which are not in agreement with the required connected flow conditions. In the present study, a floating 3 h time span of the measured aerosol number concentrations time-centred around the specific point of time was used for the COD calculation at a certain time.

ACPD
14, 1861–1917, 2014

For the investigation of connected flow, two specific particle diameter bins of the SMPS number size distribution were used. The particle number density in the 49 nm diameter bin (N_{49nm}) was selected because this represents the upper range of the aerosol particles that tend to be unaffected by cloud activation. Meanwhile, these particles tend to be substantially less affected by coagulation and diffusion processes than smaller particles. In the case of connected flow, one would expect low COD values for this parameter. The particle number density in the 217 nm diameter bin (N_{217nm}) was used to assess the likelihood of particle activation in cloud. Particles of this size are very likely to be activated in the presence of a cloud, and thus disappear from the interstitial aerosol. Thus, larger COD values for this size bin were used as a criterion to distinguish between fog and no fog conditions at the three sites in addition to the measured liquid water content at summit site. The calculated CODs for the different pairs of the three measurement sites and the two aerosol particle size bins are presented in Sect. 3 and given in table form in the Electronic Supplement (ESM).

2.3 Characterisation of the local flow connectivity using measured ozone concentrations

Besides the before mentioned aerosol particle size bins, the flow over the mountain range can be additionally investigated by locally measured trace gas concentration profile analyses. For those analyses, a quasi-chemical-inert tracer had to be used which is almost not affected by fast chemical decay and deposition throughout the travelling, and which is highly variable in time and space. In former hill cap cloud campaigns, e.g. the Great Dun Fell experiment (Colvile et al., 1997) and FEBUKO experiment (Herrmann et al., 2005), ozone has been shown to be an appropriate quasi-chemically-inert tracer. Ozone is only secondarily produced in the troposphere and has no primary direct emission sources. Moreover, ozone is characterised by low water solubility with a Henry's Law constant of about $1.0 \times 10^{-2}\,\mathrm{M\,atm^{-1}}$ (see Sander, 1999 and references therein) and is consumed only ineffectively in acidic continental clouds. Overall, the suitable properties of ozone allow the applicability of ozone as a quasi-inert tracer for

ACPD
14, 1861–1917, 2014

the connected flow analysis. Ozone concentrations were measured during HCCT-2010 at all three measurement sites with a high time-resolution by means of a TE49C-TL (up-/downwind site) and an APOA360 (summit site) gas monitor. The measured concentrations are presented in Sect. 3. A connected flow analysis based on ozone comprises a comparison of the concentration profiles regarding the concurrency of the ozone concentration levels and temporal behaviour as well as their dependency on the local meteorological conditions. In order to compare different concentration profiles and to investigate the flow connectivity in detail, the CODs of the different sites were also calculated using the measured ozone data. However, it is noted that the existing time lag between the three sites, in case of connected flow conditions, were not considered in the analysis. Low COD values indicate a good concurrency of the two ozone concentrations time series. For the COD calculation of a certain time, a time-shifted 1 h time span of the measured ozone concentrations time-centred around the specific point of time were used. The calculated ozone CODs are presented in Sect. 3 and given in table form in the ESM.

Due to the fact that the time lag between the measurements, which is mostly correlated with wind speed, is not considered in the COD analysis and the pattern of the concentration profiles are less important for COD analysis another statistical measure, the cross correlation r_{xcor}, were additionally used to assist the characterisation of the flow connectivity between the different sites. The cross correlation can be used to compare two different time series which cover the same time span. For two time series x and y, the cross-correlation value at lag time d is defined by

$$r_{\mathrm{xcor}}(d) = \frac{\sum_i \left(\left[x_i - \overline{x}\right] \cdot \left[y_{i-d} - \overline{y}\right] \right)}{\sqrt{\sum_i \left[x_i - \overline{x}\right]^2} \cdot \sqrt{\sum_i \left[y_{i-d} - \overline{y}\right]^2}} \quad (2)$$

As can be seen from Eq. (2), the cross correlation value depends on the time lag between the different time series. The time lag with the highest r_{xcor} value enables to draw conclusions on the air parcel transport time between the two stations. Moreover,

ACPD
14, 1861–1917, 2014

high correlations between the measured concentration profiles and congruent ozone concentrations time series indicate a connected flow between the sites as well as only a slight mixing with surrounding air during air parcel advection. The calculated r_{xcor} for selected time periods are presented in the ESM for each of the finally selected FCEs/NCEs.

2.4 Characterisation of the flow conditions with non-dimensional parameters

Non-dimensional flow and stability parameters such as the Froude number (Fr) and the Richardson number (Ri) can be used to characterise the flow regime in mountainous terrain exclusive of numerically expensive models. Advantageously, such parameters can be easily derived from locally measured meteorological data. In the literature, there are numerous quantities termed as Fr number, which have dissimilar forms and dynamical significance (see Baines, 1995 for details). In the present paper, the Fr number considered is defined as

$$\mathrm{Fr} = \frac{NH}{U} \tag{3}$$

in Pierrehumbert and Wyman (1985) in order to characterise whether an air mass will be lifted up and pass over a mountain, or be forced to stream around a mountain barrier. As can be seen from Eq. (3), the Fr number represents the ratio of the atmospheric potential energy, which is related to the Brunt–Väisälä frequency N times the maximum mountain height H, to the kinetic energy of the air flow represented by the characteristic wind speed U of the incoming air flow. The direct proportionality of the Fr number to the atmospheric stratification represented by the Brunt–Väisälä frequency implies that under stable stratification conditions of the boundary layer, the Froude number tends to larger values for a given wind velocity. Under both highly stable stratified conditions and/or low wind speeds, higher Fr number relates to blocking effects. Performed model simulations by Pierrehumbert and Wyman (1985) have revealed three critical Froude numbers: For Fr numbers larger than 0.75 a disturbance propagates upstream with

ACPD
14, 1861–1917, 2014

time resulting in a decelerated low-level flow, where gravity waves initiate to amplify. For larger Fr numbers ($Fr \geq 1.5$), an occurrence of a stagnant area at the low upstream slope was modelled. Simulations with even larger Fr numbers ($Fr > 2$) show a fully blocked flow pattern with a stagnant area at the upstream slope, which further extends vertically with increasing Fr values. The theoretical findings of the numerical modelling have been validated by both laboratory experiments (Baines, 1995) and in tracer studies (Bruintjes et al., 1995; Vosper et al., 2002). It is noted that the Fr formulation mentioned above assumes a dry adiabatic lifting of the airflow. Advanced investigations of Jiang (2003) and Colle (2004), taking into account additionally the formation of clouds and the associated release of latent heat, have revealed that critical Fr, where formation of stagnation pattern initiates, is about 30 to 100 % higher compared to the dry case. However, due to the uncertainties in determining the variable amount of latent heat release only the "dry" Froude number will be used hereafter.

Another dimensionless parameter characterising the stratification with respect to blocking effects represents the Richardson number (Ri), which is defined as follows:

$$Ri = \frac{g \frac{\delta \theta}{\delta z}}{\theta \left(\frac{\delta U}{\delta z} \right)^2} \quad (4)$$

The Ri number reflects the ratio of the energy extracted by buoyancy forces to the energy gained from the wind shear. In Eq. (4), g and θ represent the gravitational acceleration and the potential temperature, respectively. Moreover, vertical gradients of the potential temperature θ and the characteristic wind speed U are considered in the formulation of Ri. The thermal stratification determines the sign of the Richardson number. The airflow is statically stable for Ri values greater than zero, statically unstable for Ri less than zero or else neutral. The airflow will become dynamically unstable for Ri numbers below a critical value of about 0.25.

For HCCT-2010, the characteristic non-dimensional flow and stability parameters, Fr and Ri, were calculated using rawinsonde data from the German Weather Ser-

ACPD
14, 1861–1917, 2014

vice Station in Meiningen (453 m a.m.s.l., provided by the University of Wyoming, http://weather.uwyo.edu/upperair/sounding.html) about 30 km upwind from Mt. Schmücke. The characteristic flow speed (U), potential temperature as well as their vertical gradients were determined by averaging between the values of summit level and Meiningen level. Furthermore, an effective mountain height of about 484 m was used for the Fr and Ri calculations. The calculated Fr and Ri numbers are given in Sect. 3.

2.5 Tracer experiments

To study the local air flow under appropriate meteorological conditions, four tracer experiments (Te) were performed during the campaign (Table 1). Sulphur hexafluoride (SF_6) was used as an inert tracer gas and released at a rate of approx. $3\,L\,min^{-1}$ from a point source (bottle) at the upwind site Goldlauter for 10–20 min. Air samples were then taken at 8 different sites along the expected air flow, including both the Mt. Schmücke summit and the Gehlberg downwind sampling sites. The locations of the sampling sites are indicated in Fig. 2 and given with geographical coordinates in Table S1 (ESM). Their selection was based on the choice of sites during the previous FEBUKO experiments (Heinold et al., 2005). For consistency, the ID numbers assigned to the sites were kept the same as in (Heinold et al., 2005). Air sampling at the sites was performed during one hour after the start of the SF_6 release with a 5 min time resolution. 10 L polyethylene bags were filled with ambient air within ca. 5 s, firmly closed, and transported to the laboratory within 24 h from sampling. Analysis of SF_6 was done by gas chromatography (GC) with electron capture detection (ECD) using a Siemens Sichromat 1–4 system. A defined amount of air was removed from the bags with a gas-tight syringe and directly injected into the GC. The detection limit of the method is 0.5 ppt, the precision is $< 1\,\%$. Further details of the method are described elsewhere (Strunk et al., 2000).

ACPD
14, 1861–1917, 2014

2.6 Detailed characterisation of the meteorological and microphysical conditions

For the examination of the local meteorological conditions during the selected FCE periods, the locally measured meteorological and microphysical data, rawinsonde observations, satellite pictures, ceilometer data and calculated backward trajectories have been used focusing on the stability of the incident flow conditions, synoptic front passages, the presence orographic or non-orographic cloudiness, measured cloud properties such as cloud base height and LWC, vertical thermal stratification and occurred precipitation.

For detection of frontal processes and the synoptic scale advection pattern, surface weather charts with a time resolution of 6 h and charts of the 850 hPa pressure level have been used (see ESM). Moreover, backward trajectories were calculated with the HYSPLIT model (Draxler and Rolph, 2003; Rolph, 2013) in order to identify the air mass origin as well as to characterise potential source region of the aerosols and homogeneity of the of advected air masses during a identified FCE. The HYSPLIT model was used in the ensemble mode in order to provide multiple backward trajectories based on a small variation in the applied initial meteorological field. The ensemble trajectory calculations were done to lower the associated uncertainties with a single trajectory and to investigate the potential variability of the calculated backward trajectories according to variations in the meteorological field. Each calculated ensemble trajectory starts from the same location, however the initial meteorological field was offset by 1 grid cell in the horizontal and by 250 m in vertical direction. So, 27 ensemble backward trajectories were calculated (see ESM). Additionally, the trajectories were analysed regarding their residence time over certain land (urban, agriculture, natural vegetation and bare areas) or water areas throughout their travelling to Mt. Schmücke in order to characterise the aerosol type and origin in more detail (see van Pinxteren et al., 2010 for details of the trajectory analysis approach).

ACPD
14, 1861–1917, 2014

For the characterisation of the cloud conditions and the thermal stratification, satellite pictures and rawinsonde observations were used. For the analyses, both IR and VIS satellite pictures of the geostationary METEOSAT satellite with 15 min time-resolution and, if available during the FCEs, polar orbit satellites pictures (source: Berliner Wetterkarte e.V., 2010 and DLR) were examined. As has been mentioned in Sect. 2.4, rawinsonde observations from the German Weather Service station Meiningen (source: http://weather.uwyo.edu/upperair/sounding.html) were analysed regarding the present tropospheric thermal stratification and vertical wind pattern. The latter facts are used to characterise vertical thermodynamic conditions for the existing clouds supporting the determination of the cloud type present at the measurement site. Moreover, the standard meteorological parameters such as temperature, pressure, relative humidity wind direction, wind speed and precipitation, which were measured at all three measurements sites by means of Vantage Pro weather stations, and used for the critical meteorological assessment. Furthermore, the cloud base height measured at the upwind site by a ceilometer (Jenoptic Ceilometer CHM 15k) and liquid water content (LWC) detected at the summit site with a both FSSP-100 and PVM-100 instrument are investigated to characterise the microphysical cloud conditions and their homogeneity throughout the FCEs. Lastly, the locally measured data assists with the detection of meteorological front passages and thus possible air mass changes. Overall, the additionally performed meteorological analysis allows an even more comprehensive evaluation and characterisation of the selected cloud periods with regards to other important meteorological issues needed for an appropriate hill cap cloud experiment besides the connected flow conditions.

ACPD
14, 1861–1917, 2014

3 Results and discussion

3.1 Characterisation of the general synoptic situation and advected air mass during HCCT-2010

The average synoptic situation during September 2010 was characterised by a weak low-pressure area between Greenland and Iceland as well as a weak high-pressure area over Romania resulting in a predominantly westerly flow over Central Europe (Fig. 3). Particularly, the second half of the month was affected by front passages and changeable weather conditions.

At the beginning of the field campaign on 14 September in 2010, at the foreside of a trough over Central Europe (TM) marine air from North Atlantic (mTp) was advected to the measurement site. The day after, the trough moved eastwards, allowing an Atlantic frontal zone to reach Central Europe leading to precipitation with occasional gusty winds. On the backside of the cold front Greenlandic polar air (mP) was advected to the Mt. Schmücke area staying until 17 September. The trajectory analysis shows that the observed air mass was mainly influenced by marine and agriculturally used areas of Great Britain or France (cp. next section). Several (partly quite short) measurement periods (see Table 2) were started despite the precipitation because of appropriate wind conditions. From 18 September on, a bridge of high pressure developed over Central Europe. Warmed maritime polar air (mPt) with decreasing oceanic influence in the course of the following week until 23 September approached the Thuringian Forest resulting in moderate winds mainly from SW. On 20 and 21 September, the wind direction shifted towards easterly directions without any change in the origin of the air mass. This confirms the finding that the influence of the continent (agriculture, natural vegetation) on the air mass highly increased with continuing time during that week (see trajectory analysis in the ESM). On 24 September, a transition occurred changing the air mass advection towards more polar characterised air mass. During the next three days (until 28 September), a strengthening low-pressure area over the North Sea induced aged Greenlandic polar air (mP) to Central Europe. The weather conditions were appropriate

ACPD
14, 1861–1917, 2014

for another offline experiment period on 24/25 September (see Table 2). The weather situation thereafter was characterised by strong precipitation connected to front passages. The subsequent weather situation from 29 September to 3 October 2010 was affected by a large High over Scandinavia and an Icelandic Low generating temporary precipitation at the corresponding fronts. The air mass was characterised by dryer and warmer air (cTp) compared to the days before together with an advection over the continent (France) from south-western directions. Two offline experiment periods were conducted during this weather situation (see Table 2).

October can be divided into 5 distinct weather periods (see Table 2). No change in the general weather situation is observed for the first three days of October compared to the last period in September. Two offline experiment periods were conducted during this weather situation (cp. Table 2). The weather situation from 4 October to 8 October was characterised by a high-pressure area over Russia and Poland and areas of low pressure over the Atlantic Ocean. The Mt. Schmücke area was in a zone of weak pressure gradients characterised with warm and humid air advected from the Mediterranean area in the South. The declining pressure gradients cause weak winds from south-westerly directions and later (from 6 October on) different directions. The marine influenced tropical air mass (mTs) causes early morning fog, yet precipitation only in Southern Germany, but not in the Mt. Schmücke area. Frontal systems are blocked in the west and south of Germany by the high over Poland and Russia. By 9 October, the weather situation changed. The high-pressure area over Poland and Russia receded and a new high-pressure area formed over the Norwegian Sea (HNA). The Mt. Schmücke area got under the influence of high pressure with early morning fog. Pressure gradients were still weak. Wind direction has changed to northerly directions advecting dry continental polar air masses. By 15 October, the general weather situation started to change and a trough area over Central Europe (TrM) influenced Mt. Schmücke from 16 October on. The trough led to an advection of humid marine polar air masses associated with occasionally occurring precipitation over Germany. From 22 October, the trough was pushed eastwards and westerly conditions (WZ) af-

ACPD
14, 1861–1917, 2014

fected the Mt. Schmücke area advecting marine air masses (mTp). During this weather situation, two offline cloud experiments were performed (see Table 2)

3.2 Flow characterisation

3.2.1 Overflow characterisation with the quasi-inert gas tracer (O_3)

As has been mentioned in Sect. 2, measured ozone concentrations time series and derived statistical parameters such as the COD and the cross-correlation can be used for the characterisation of the flow connectivity between the different sites and finally for the revelation of suitable experimental periods, which will allow further investigations. The measured ozone concentrations at the three sites and the different calculated COD values based on ozone are presented in Fig. 4 together with important meteorological data such as wind speed and direction. The plot shows that the ozone concentrations at the different sites are quite variable in space and time. The short-range variability of the concentration pattern represents the good precondition for the statistical analysis. The ozone concentrations vary between few ppb and about 60 ppb. The depiction of the ozone concentrations reveals mostly quite good congruencies between the measured data of the summit and downwind site. The concentration time profile of the upwind site shows larger deviations in comparison to the others. Strong congruencies between the measured ozone concentration profiles are mostly present for weather situations with south-western or west-south-western flow conditions. Rather good flow connectivity, i.e. strong congruencies, is also found for weather situations with north-eastern winds perpendicular to the mountain ridge. Moreover, it can be seen from Fig. 4 that congruent periods are mostly also associated with higher wind speeds reflecting the higher kinetic energy of the airflow and the higher probability for the air to cross a mountain range. The most congruent time intervals are shaded in Fig. 4. The comparison of the concentration-time profiles and the calculated CODs shows that larger deviations between the different time series coincide directly with the higher CODs. The COD analysis reveals mostly higher CODs for calculations, which considers up-

ACPD
14, 1861–1917, 2014

wind site data. This result is in agreement with the above-mentioned findings, which have found mostly a stronger correlation between the summit and downwind measurements and more often a potentially disconnected flow. The average of the $COD_{GB\text{-}SM}$ throughout the analysis period is with about 0.11 smaller than the COD averages of the two other combinations ($COD_{SM\text{-}GL}/COD_{GB\text{-}GL}$: 0.13/0.16).

Figure 5 shows a histogram of the ozone CODs for the different station combinations. For the CODs of the summit and downwind site ($COD_{GB\text{-}SM}$), a higher number of smaller CODs are calculated reflecting the mostly higher correlations between them compared to the 2 other combinations. It can be seen that more than 60 % the CODs of ozone (GE/GL) are smaller than 0.15. Moreover, the investigations of the different concentration-time series have revealed good congruencies between the measured profiles for CODs up to 0.1 and still acceptable congruencies for CODs up to 0.15. For larger CODs, larger deviations have been observed, which correspond to a potential disconnection of the flow between the field sites. Based on this subjective finding, a qualitative assessment of the conditions was done based on the derived ozone COD dataset in order to separate suitable and unsuitable time periods. To assess and separate specific conditions, five different assessment criteria were used: (1) for COD $\leq$ 0.05 (very good correlation), (2) for CODs of 0.05 $\leq$ COD $\leq$ 0.1 (still good correlation), (3) for CODs of 0.1 $\leq$ COD $\leq$ 0.15 (small correlation), (4) for CODs of 0.15 $\leq$ COD $\leq$ 0.2 (poor correlation) and (5) for CODs of 0.2 $\leq$ COD (very poor or no correlation). For the overall assessment of the flow connectivity, other parameters are additionally considered, thus, the results are hence summarised in Sect. 3.5.

The additionally performed cross correlation analyses using the measured ozone concentration profiles at the different sites have revealed similar findings than the COD analyses. The cross correlation plots for the finally selected experimental periods are presented for the sake of clarity in the ESM. Figure 5 shows exemplarily a plot for a selected experimental cloud period. The three lines in Fig. 5 represent the calculated cross correlation between the different sites for different time lags. The plot reveals rather high cross correlations with r_{xcor} values of about 0.7 to 0.9 reflecting the po-

ACPD
14, 1861–1917, 2014

tentially high flow connectivity between all sites throughout this time period. Moreover, Fig. 5 displays the highest correlations between zero and −20 min time lag. This finding implies that the air transport time, e.g. from the summit to the downwind site (green line in Fig. 5) should be on average about 10 min during this selected period. The overall mean transport time between upwind and downwind site during this time period should be about 20 min due to the maximum of the cross correlation at this time lag. As similarly obtained by the COD analysis, the correlations between the summit and the downwind site are usually somewhat higher compared to the other combinations including the upwind site data. Additionally, it should be noted that transport times can considerably vary throughout the finally selected experimental periods. Therefore, the cross correlation plots for both the whole selected period and shorter time intervals (mostly 3 h) are given in the ESM. The individual results of the cross correlation analyses for each of the finally selected periods of the overall assessment are summarised in Sect. 3.5.

3.2.2 Overflow characterisation with aerosol particle distribution data

Besides ozone, two aerosol particle size bins of the SMPS were used for the assessment of the flow connectivity between the different sites and the prevailing cloud conditions. The measured number concentrations at the three sites and the corresponding three COD values are presented in Fig. 4. Figure 4 shows that the N_{49nm} and N_{217nm} concentrations at the different sites are highly variable so that they permit the application of COD analyses.

The N_{217nm} plot reveals mostly quite good congruencies between the measured data of the upwind and downwind site. Number concentrations (N_{217nm}) of the summit site show partly larger differences. As can be seen from the plot, the N_{217nm} bin always shows very low concentrations in the presence of clouds or fog due to CCN activation in this size range. This behaviour leads to large COD values ($COD_{N217nm} > 0.8$) during periods, where a cloud is present at the summit site and non-cloud conditions in the valleys. Thus, this parameter is suitable to characterise cloud/fog conditions at the dif-

ACPD
14, 1861–1917, 2014

ferent sites and to differ between flow conditions with and without cloud interaction. To separate time intervals with or without cloud (with/without activation of the accumulation mode particles), a COD_{N217nm} criterion was defined in addition to LWC measured at Mt. Schmücke. For COD_{N217nm} values are larger than 0.4 activated accumulation mode particles, i.e., cloud/fog conditions are expected.

The measured N_{49nm} bin data of the three sites show mostly quite similar concentration pattern. The calculated COD_{N49nm} shows the lowest values during weather situations with both south-western and north-eastern winds indicating rather good flow connectivity. The comparison of the N_{49nm} bin concentration-time profiles and the calculated CODs shows that larger deviations between the different concentration profiles coincide directly with higher COD_{N49nm} values. Larger COD_{N49nm} values are often in agreement with COD_{O3} findings. However, it is noted that the time series of the COD_{N49nm} show larger noise pattern probably due to the coarser time resolution of the input data and a lower variability compared to the COD_{O3} values. Overall, the investigations of the different N_{49nm} bin concentration-time profiles have revealed that reasonable congruencies between the measured profiles exist for CODs up to 0.2. For larger CODs, larger deviations were present and thus a potential disconnection of the flow between the field sites most likely exists. Based on this finding and former studies (see Sect. 2), a qualitative assessment of the conditions was done using the COD_{N49nm} dataset to separate time periods with and without connected flow conditions. In order to assess and separate specific conditions, five different assessment criteria were applied: (1) for $COD_{N49nm} \le 0.05$ (very good correlation), (2) for $0.05 \le COD_{N49nm} \le 0.1$ (good correlation), (3) for $0.1 \le COD_{N49nm} \le 0.15$ (reasonably good correlation), (4) for $0.15 \le COD_{N49nm} \le 0.2$ (small correlation) and (5) for $0.2 \le COD_{N49nm}$ (very poor or no correlation). The COD_{N49nm} dataset is presented in table form in the ESM. The different COD_{N49nm} values are presented there with a predefined colour code for classification of the connected flow and cloud conditions (see ESM for details). These results were used for the selection of the most suitable investigation periods (see next section).

ACPD
14, 1861–1917, 2014

Moreover, for the overall assessment of the flow connectivity, other parameters are additionally considered, thus, the overall assessment is outlined in Sect. 3.5.

3.2.3 Selection of potentially suitable investigation periods

The main goal of the present study was the quantitative identification of the most appropriate periods, where connected flow conditions between the three measurement sites were present. Based on the above-mentioned statistical measures (e.g., COD_{O3}, COD_{N49nm}, etc.) both cloud periods and no-cloud periods with suitable connected flow conditions should be identified in a objective and automatic manner according to a successive procedure based on predefined criteria. The aimed Full-Cloud-Events (FCE), i.e. periods with connected south-westerly flow conditions and cloud conditions present only at Mt. Schmücke (summit site), and Non-Cloud-Events (NCE), i.e. periods with connected south-westerly or north-easterly flow conditions and non-cloud conditions at any site, were identified following the section procedure shown in Fig. 6.

As can be seen from Fig. 6, cloud (COD_{N217nm}/LWC) and precipitation (RR: precipitation rate of the last 30 min) criteria were applied in addition to the flow criteria in order to obtain adequate NCEs and FCEs. The latter are expected to be characterised e.g. by clouds with an appropriate Liquid Water Content (LWC) and CCN activation as well as almost no rain-out. The quantitative identification of the FCEs and NCEs was done with a two-step procedure. As shown in Fig. 6, at first the flow criteria, described in the subsections above, were applied leading to the identification of suitable periods with connected flow condition (SW/NE wind sector). In the second step, the cloud conditions were evaluated using, e.g., the measured LWC at the Mt. Schmücke. Moreover, the CODs of the aerosol number concentration bin (N_{217nm}), activated CCN bin under typical cloud/fog conditions) were used to both identify cloud/non-cloud conditions at the summit and exclude conditions with fog at the valley sites. Therefore, suitable NCEs have been identified with connected overflow conditions both with SW and NE winds. For the quantitative identification of the most appropriate FCEs additionally the amount of precipitation at the sites were evaluated and only periods with insignificant amount of

ACPD
14, 1861–1917, 2014

precipitation were selected. The whole dataset including meteorological data, the different calculated CODs and finally a table with the identified FCEs and NCEs are given in the ESM. The different parameters are presented there with a predefined colour code for classification of the connected flow and cloud conditions (see ESM for details). A brief summary of the most important parameters (mean CODs, etc.) of the selected FCEs is given in Table 3. It is noted that the selected FCEs are listed in chronological order without a classification. A final evaluation of the FCEs including also other issues is made in Sect. 3.5. Moreover, it is noted that the corresponding table for the selected NCEs is given in the ESM.

For the different FCEs, a nomenclature has been used, which refers to the chronological occurrence of prolonged cloud periods during HCCT-2010. The occurred cloud periods, which could be also characterised by small breaks, i.e. conditions with LWC values close to zero, were determined based on the measured time series of LWC at Mt. Schmücke and numbered chronologically. Moreover, the defined cloud periods themselves were subdivided into specific uninterrupted cloud event periods, i.e. without very low LWC values (continuous cloud conditions). As an example, the selected event FCE1.1 refers to the first (uninterrupted) part of the first prolonged cloud period occurred at Mt. Schmücke during the campaign.

3.2.4 Overflow characterisation with non-dimensional parameters

The calculated Froude numbers (Fr) and the Richardson numbers (Ri) for the different rawinsonde observations (from Meiningen approximately 30 km upwind of Mt. Schmücke) during or near the selected FCEs/NCEs (with SW flow conditions only) as well as associated remarks are listed in Table 4. As can be seen from Table 4, in many cases no blocking or only a slightly decelerated flow is present. Only in some cases, the Fr number analysis predicts a stagnant flow or area. The calculated values show that the flow conditions are mostly determined by the atmospheric stratification and in some cases also by the wind speed conditions. Larger Fr numbers coincide always with high Ri numbers indicating very statically stable conditions. However, also

ACPD
14, 1861–1917, 2014

under stable conditions, as observed on 14 September 2010 14:00 CEST, acceptable flow conditions for the air to cross a mountain can be achieved due to high means wind speeds ($8\,m\,s^{-1}$). On the other hand, the small Fr numbers and negative Ri numbers for example on 19 September 2010 14:00 CEST imply no present blocking at this time. The comparison of the calculated non-dimensional parameters with the calculated COD values of ozone and the 49 nm size bin (hourly average for COD between the up and downwind site) shows a rather good agreement. Higher Fr and higher Ri numbers, which indicate a potential blocking of the airflow, coincide mostly with higher COD values reflecting deviations between the different sites. For example in case of the chosen event FCE11.3, the Fr number calculated from the rawinsonde data of the 2 October 2010 (14:00 CEST) indicates with a value of 0.81 a still possible air flow over the mountain range, whereas the calculated Fr (1.31) and Ri number (7.19) of the 3 October 2010 (02:00 CEST) imply a stronger deceleration of the flow under very stable conditions. This result is confirmed by the COD analysis, which reveals with ozone CODs larger than 0.2 rather high values after half past midnight. A similar behaviour can be obtained for FCE13.3, where better flow conditions are predicted by the Fr number for the daytime observation (6 October 2010, 14:00 CEST: Fr = 0.85 and COD_{O3} = 0.09 and COD_{N49nm} = 0.12) compared to the subsequent night-time observation (7 October 2010 02:00 CEST: Fr = 1.16 and COD_{O3} = 0.14 and COD_{N49nm} = 0.27), where a disconnection between the upwind and the two seems to be present after 01:00 CEST (see Table 4, and the time-resolved COD analysis data in the ESM). From the selected FCEs, the present investigation using Fr and Ri number shows good flow and stability conditions for the FCE1.1, FCE26.1 and FCE26.2. Finally, it is noted that due to the focus of the present study on the FCEs, the Fr and Ri numbers related to the NCEs are not discussed here in detail.

3.3 Detailed meteorological characterisation of the selected FCEs

In the following, the results of the detailed meteorological examination of the selected FCEs are outlined. The selected FCEs were investigated with respect to the separa-

ACPD
14, 1861–1917, 2014

tion of orographic and non-orographic clouds, the detection of frontal processes, the stability of air mass advection (local/synoptic scale) and the cloud conditions (LWC, precipitation, cloud base height) by means of on locally measured meteorological and microphysical data, rawinsonde observations, satellite pictures, ceilometer data and calculated backward trajectories.

3.3.1 FCE1.1 (start: 14 September 2010 11:00 CEST, end: 15 September 2010 01:50 CEST)

The first cloud event FCE1.1 lasted for about 15 h. Starting at 11:00 CEST, the weather situation at the experimental site was characterised by a warm front of a low-pressure system near Iceland bringing slight precipitation (RR < 1 mm) to Mt. Schmücke during the first hour of the measurement. In the course of the event, the Low moved south-eastwards leading to a continuously decreasing air pressure at the measurement site. The cloudiness occurring at the summit cannot be labelled as a pure orographic cloud since high clouds covered the area permitting no clear statement. Nevertheless, an orographically induced cloud that was only observed at the summit cannot be excluded since air was advected continuously from WSW to Mt. Schmücke leading to ideal wind conditions with a consistent wind speed of about 8.2 $m\,s^{-1}$ and stable stratification throughout the whole cloud event. The liquid water content decreased from 0.45 to 0.15 $g\,m^{-3}$ over the measurement time, conforming to the relative humidity measured at the upwind site, which also decreased. Furthermore, the cloud base height decreased from 150 m above ground at 11:00 CEST to 70 m at 13:00 CEST and increased again afterwards to about 280 m at 21:00 CEST. This corresponds to the findings of the rawinsonde, which indicate a general increasing cloud base height. Within the following 3 h, the cloud base height fell dramatically to 130 m above ground. Afterwards, high fluctuations in the cloud base height were observed at the measurement site indicating slight precipitation (RR < 1 mm) that occurred close to midnight for about 1.5 h as the cold front of the low-pressure system approached to the measurement site. The calculated backward trajectories and corresponding trajectory analysis (see Fig. 7 and the corre-

ACPD
14, 1861–1917, 2014

sponding Figures in the ESM) indicate that the air mass was advected in a cyclonic bend and was (time-wise) in nearly equal shares characterised by the North Atlantic as well as agricultural and natural vegetation regions in Western Europe during the measurement period. Also a small urban influence, e.g. due to the passage of Paris, is possible.

3.3.2 FCE1.2 (start: 15 September 2010 03:00 CEST, end: 15 September 2010 06:20 CEST)

Strong postfrontal advection of Greenlandic polar air (mP) introduced a cyclonic west circulation at Mt. Schmücke and led to temporary cloud dispersal. But the following rather short cloud event (duration: 3 1/3 h) was again characterised by slight precipitation ($RR < 0.4$ mm at all sites), increasing LWC from 0.05 to 0.28 $g\,m^{-3}$ as well as slightly stable thermal stratification. The wind blew steadily from SW (231°) with moderate wind speeds of 9.6 $m\,s^{-1}$. The air mass was mainly advected over the North Atlantic Ocean and agriculturally used areas (see Fig. 7). During the event period, the cloud base height continuously changed between 150 and 300 m.

3.3.3 FCE2.1 (start: 15 September 2010 23:00 CEST, end: 16 September 2010 02:00 CEST)

Due to the cyclonic west circulation, Greenlandic polar air (mP) was slowly advected to the measurement site resulting in smaller but slightly increasing wind speeds of about 8.7 $m\,s^{-1}$ from WSW (240°) during FCE2.1 (duration: 3 h). The air mass mainly crossed the English Channel and Northern France indicating smaller continental impact (see Fig. 7). From 23:00 CEST on, the cloud base height decreased from 380 to 280 m above ground and increased again during the event to 420 m. The LWC showed a maximum at midnight of 0.25 $g\,m^{3}$, decreasing in both directions to about 0.05 $g\,m^{-3}$. The satellite images imply that the present cloud was probably not purely orographically induced, but advected by the large-scale westerly flow over Central Europe. No

ACPD
14, 1861–1917, 2014

precipitation occurred during the three hours of the selected cloud event and stable stratification occurred.

3.3.4 FCE4.1 (start: 16 September 2010 13:10 CEST, end: 16 September 2010 15:00 CEST)

During the day of 16 September, the general weather situation did not change distinctively. The occlusion of a small low-pressure system over the Skagerrak brought slight precipitation (RR < 0.8 mm) to the site during the event (duration: 2:50 h). The cloud base height changed from 350 m to a lower cloud (150 m) occurring at Mt. Schmücke around 12:00 CEST and cloud dissipation as well as stopping precipitation at the end of the measurement. The wind speed of about 7.4 $m\,s^{-1}$ decreased somewhat throughout the event coming from slightly changing directions of SW (220°) to WSW (250°), conforming to rather unstable backward trajectories that originate in Atlantic regions from the Arctic cycle to the Azores. The rawinsonde data indicate a labile thermal stratification. The LWC decreased from about 0.2 to 0.1 $g\,m^{-3}$ throughout the cloud period.

3.3.5 FCE5.1 (start: 16 September 2010 21:40 CEST, end: 16 September 2010 23:50 CEST)

In the evening of the same day another experimental period started (duration: 2:10 h). Still high-reaching cold marine air (mP) approached Mt. Schmücke in a cyclonic manner. Slightly smaller wind speeds were observed (6.3 $m\,s^{-1}$) from WSW (240°). The cloud base height was 150 to 250 m above ground with constantly high LWC in the cloud of 0.3 $g\,m^{-3}$ during the event. No precipitation occurred. The trajectory analysis indicates a mainly oceanic influenced air mass and rather unstable trajectories originating from westerly directions. The analysis of the rawinsonde data indicates that the lower atmospheric layers were slightly stable stratified.

ACPD
14, 1861–1917, 2014

3.3.6 FCE7.1 (start: 24 September 2010 21:10 CEST, end: 25 September 2010 00:50 CEST)

During the day, the general weather situation changed from high-pressure conditions to a cyclonically characterised weather situation. The strengthening low-pressure system over the North Sea advected aged Greenlandic polar air (mP) to the measurement site leading to wind speeds of 5–8 $m\,s^{-1}$ from WSW (228°) at Mt. Schmücke. Based on the trajectory analysis (see Fig. 7), the advected air mass was mainly characterised by natural vegetation and to smaller amounts by agricultural land use and water surfaces resulting form the fast advection of the air mass during the last 96 h mainly over France and partly from the Eastern Atlantic to the measurement site. Under stable thermal stratification conditions, an orographic cloud (see Fig. 8) occurred at the summit with a cloud base height of about 220 m above the upwind site and an increasing LWC of 0.1 to 0.3 $g\,m^{-3}$. No precipitation was observed during the event of 3:40 h duration.

3.3.7 FCE11.2 (start: 1 October 2010 20:50 CEST, end: 2 October 2010 03:10 CEST)

The weather conditions during this period (duration: 6:20 h) were characterised by an occlusion prior to the frontal system of a low-pressure system over the North Atlantic that only becomes important for the next event. The occlusion could barely move north-eastwards because of the blocking anticyclone over Scandinavia. The air mass was mainly continentally influenced and fast advected over France passing both agriculture and natural vegetation areas. The measured wind data at Mt. Schmücke showed a stable south-westerly flow (222°) with comparably low wind speeds of 3.7 $m\,s^{-1}$. The observed cloud at the summit was characterised by a changing the base height from 120 to 200 m. The cloud type cannot be confirmed for sure, but an occlusion-related cloud seems plausible. The LWC doubled from 0.25 to 0.5 $g\,m^{-3}$ throughout the experiment and no precipitation was observed.

ACPD
14, 1861–1917, 2014

3.3.8 FCE11.3 (start: 2 October 2010 07:10 CEST, end: 3 Ocotber 2010 00:30 CEST)

2 October was characterised by a low depression (965 hPa) over south of Iceland advecting continental tropical air from south-west (220°) to the measurement site with varying wind speed of 4–9 $m s^{-1}$ (max. at 17:00 CEST). At the beginning of the experiment, i.e. the first 1.5 h, the warm front caused slight precipitation (RR < 0.5 mm) at Mt. Schmücke. The cloud base height varied between 100 and 250 m at a constant LWC of 0.32 $g m^{-3}$. RH slightly increased from 96 % to 98 % at the upwind site. The air mass was permanently influenced by agriculturally used areas or natural vegetation. Since also higher clouds occurred at the measurement site, the type of the lower level cloud cannot be confirmed for sure, but a partly orographically induced cloud is possible (see ESM). The rawinsonde data shows stable thermal stratification throughout the event. The experiment lasted for 17:20 h and provides overall adequate conditions.

3.3.9 FCE13.3 (start: 6 October 2010 06:50 CEST, end: 7 October 2010 01:00 CEST)

An extended measuring period with good meteorological conditions was on 6/7 October. The cloud event lasted 15 h. The weather situation during that time was characterised by a high over Russia and a low-pressure area over Iceland. The Schmücke area stayed in a sector of warm air with weak pressure gradients causing low wind speeds less than 4 $m s^{-1}$ at Mt. Schmücke. During the measuring period, the high-pressure system extended slowly into the Schmücke area and the sector of warm air diminished gradually. The backward trajectory analysis (see ESM) shows a large scattering between the different ensemble runs. Depending on the starting point of the trajectory, there is a high variability in the direction of the trajectory reaching from south-easterly over southern and western to north-easterly directions. Therefore, it cannot clearly be verified whether the air mass was more marine or continental influenced. The most likely trajectory moved westerly from the Atlantic Ocean towards the UK,

ACPD
14, 1861–1917, 2014

then made a loop over the Bay of Biscay and approaches the Schmücke area from the southwest passing France. The south-western airflow was stable throughout the whole selected period. The rawinsonde data shows rather stable thermal stratification conditions throughout the event. From the VIS satellite pictures, an orographic cloud effect can be clearly seen. A bank of cloud filled wide regions of Thuringia and Bavaria and a sharp edge is seen at the mountain ridge of the Thuringian Forest (see Fig. 9). The cloud height varied between 100 and 200 m throughout the cloud event. The cloud was characterised by high LWC values between 0.3 and 0.55 $g\,m^{-3}$ except for a short period between 11:00, and 15:00 CEST, where the LWC decreases to values down to 0.1 $g\,m^{-3}$ (mean LWC 0.32 $g\,m^{-3}$).

3.3.10 FCE22.0 (start: 19 October 2010 01:50 CEST, end: 19 October 2010 09:00 CEST)

During this 7 h period, the Schmücke area lied in a trough while a high-pressure bridge began to build up in the South of Germany. Temperatures stayed constantly below the freezing point during the period. There was an occlusion directly over the Schmücke area. Moreover, a cold front from a low-pressure system with centre over southern Norway passed Mt. Schmücke at the end of the measuring period bringing light precipitation and low clouds. The cloud event was characterised by constant south-western flow conditions (mean wind direction: 233°) with moderate wind speeds (mean: 5.1 $m\,s^{-1}$) and LWC levels around 0.2 $g\,m^{-3}$. The rawinsonde data shows rather stable thermal stratification conditions. The cloudiness at Mt. Schmücke was caused by the occlusion and frontal system rather than by pure orographic lifting. The backward trajectory analysis (see ESM) shows a large scattering between the different ensemble runs. In general, most of the trajectory shows an advection of cold air from northern directions to the North of France and a subsequent south-western advection to the experimental area. Moreover, the backward trajectory analysis revealed that the arriving air mass was mainly continentally influenced and has passed mainly both agriculture and natural vegetation areas.

ACPD
14, 1861–1917, 2014

3.3.11 FCE22.1 (start: 19 October 2010 21:10 CEST, end: 20 October 2010 02:30 CEST)

There were slight changes in the synoptic situation compared to the event FCE22.0. Germany has become more influenced by low pressure with the centre of the low-pressure system over Germany. Moderate winds were present at Mt. Schmücke, which periodically tend to be too westerly for an ideal setup of the experiment. The general wind direction at Mt. Schmücke changed towards westerly direction (around 260°), e.g. to the upper limit of the predefined wind sector. The analysis of the backward trajectories shows stable westerly flow conditions for most of the ensemble members. Due to the westerly advection, the air mass passed both by both maritime and continental (agriculture/natural vegetation) areas. The data of the rawinsonde shows slightly stable thermal stratification conditions. The measured LWC increased from 0.18 to 0.3 $g\,m^{-3}$ within the first 30 min and stayed rather constantly around that value afterwards with slightly higher values at the end of the period around 0.37 $g\,m^{-3}$. The cloud height from the ceilometer data in Goldlauter varies between 100 and 190 m, whereas the relative humidity at the upwind site stayed rather constant. On the IR satellite images (see ESM), dark-grey and uniform areas can be mostly seen, which indicate the presence of lower stratiform cloudiness at the experimental site.

3.3.12 FCE24.0 (start: 21 October 2010 22:10 CEST, end: 22 October 2010 10:00 CEST)

The general synoptic situation was characterised by a high-pressure area in the south of Germany and a low-pressure system passing Denmark and the South of Sweden. The measurement area lied in a frontal zone with somewhat stronger pressure gradients causing mean wind speeds up 6 $m\,s^{-1}$ from south-western directions (mean 241°) at Mt. Schmücke ideally for the experimental design. The analysis of the backward trajectories shows for all ensemble members stable advection from Greenland to France and subsequently to the measurement site. Due to the advection path, the air mass

ACPD
14, 1861–1917, 2014

passed both by both maritime and continental (agriculture/natural vegetation) areas (see Fig. 7). The data of the rawinsonde shows quite stable thermal stratification conditions (see ESM). There was a cloud throughout the whole period with LWC values between 0.04 and 0.25 $g\,m^{-3}$. It is noted that no offline sampling was performed as the temperature was below the freezing point. Most of the available IR satellite images (see ESM) illustrate a dark-grey and uniform cloud orographic pattern that indicate a relative warm cloud top and thus lower stratiform cloudiness at Mt. Schmücke. Furthermore, slight precipitation (RR_{SM} = 0.14 mm) was observed during the event, which last for nearly 12 h duration.

3.3.13 FCE26.1 (start: 23 October 2010 23:40 CEST, end: 24 October 2010 07:20 CEST)

During FCE26.1 a low pressure system passed the Schmücke area. The centre over Great Britain and the North Sea moved quickly to northern Germany, Denmark and southern Sweden. Initially, the Mt. Schmücke area lied in the warm sector of the low-pressure system. The cold front passed the experimental site bringing light precipitation between 00:30 and 03:00 CEST. Postfrontal precipitation has been also observed around 05:30 CEST. The analysis of the trajectories shows a high variability in the course of the distinct ensemble members. The analysis of the trajectory residence times shows that the air mass was advected over both maritime and continental areas. The wind blew from south-westerly directions. The wind speed, however, was quite high with mean wind speeds up to 13 $m\,s^{-1}$ at the beginning of the cloud period. The data of the rawinsonde shows only less stable thermal stratification conditions. The LWC gradually increased from 0.07 $g\,m^{-3}$ to about 0.2 $g\,m^{-3}$ within the first hour and stayed almost constant thereafter. The cloud height decreased from 300 m to 160 m within the first two hours, varies between 230 and 130 m until the end of the measuring period. However, due to the frontal system, a pure orographic cloud cannot was not present. Light precipitation caused an interruption of the measuring period until 08:40 CEST, where the FCE26.2 were started.

ACPD
14, 1861–1917, 2014

3.3.14 FCE26.2 (start: 24 October 2010 08:40 CEST, end: 24 October 2010 12:20 CEST)

After the passage of the cold front, wind speed remained high at values around 9 $m s^{-1}$ still from south-westerly directions. The LWC decreased from about 0.2 to 0.06 $g m^{-3}$. The cloud base is found at about 200 m throughout the measuring period and is lifted to 350 m with the last hour of the measurement period. Light postfrontal precipitation was observed between 10:50 and 11:40 CEST. The analysis of the trajectories shows a significant variability with half of the ensemble members coming from western directions and half of the members coming from northern directions.

3.4 Tracer experiments

The SF_6 tracer experiments were carried out during the campaign when local meteorological conditions seemed favourable. The post-campaign in-depth analysis of flow connectivity between the sites revealed, however, that only during two of the experiments (TE1 and 3, see ESM) upwind and downwind sites can be compared in a Lagrangian-type approach. TE1 falls within the validated NCE0.4, while TE3 is part of FCE13.3 (see previous section).

During TE2 and TE4, the COD analyses indicated poor flow connectivity between the sites (see Table 1). Thus, only the results of TE1 and TE3 are shown in Fig. 10. Different pathways of the plume can be observed during the two experiments, related to the dominant wind direction during the experiments. During TE1 the wind direction at the in-cloud site had a higher westerly component (mean dd_{SM} of 240°, cf. Table 1) than during TE3 (mean dd_{SM} of 220°). Accordingly, during TE1 the plume passed more over the sampling sites to the East of the release site, observed by higher mixing ratios of the sites 22, 42, and 32 as compared to their western counterparts 21, 41, and 31. The opposite was observed during TE3, where the western sites 41 and 30 caught larger parts of the SF_6 plume. Site 21 showed somewhat lower concentrations than its eastern counterpart 22. However, SF_6 peaked rather late at site 22, even later than at the more downwind Mt. Schmücke site (20). This indicates that is was likely not part of the main pathway of the plume.

During both TE1 and 3, the highest SF_6 mixing ratios were usually observed at Mt. Schmücke (ca. 110 ppt). Due to diffusion and dilution lower values are observed at the downwind sites, which were, however, still well-observable at about 30–60 ppt. This shows that the assumption of a connected air flow along upwind, summit, and downwind sites was indeed valid during these experiments. Even though during TE3 the SF_6 plume did not directly pass the official Gehlberg downwind site (32), it seems valid to assume that during the FCEs (and NCEs) – when spatially more homogeneous aerosol passes the area rather than a plume originating from a point source - representative air parcels can be sampled at the Gehlberg site as long as the wind direction falls within the valid corridor.

The time difference between the start of the SF_6 release and its peak mixing ratio at one of the two downwind sites (30 or 32) was 30 min for TE1 and 45 min for TE3. The mean wind speed at the Schmücke was about twice as high during TE1 as during TE3 (Table 1), which qualitatively agrees with the quicker travelling time. It has to be noted that in both experiments the SF_6 likely needed some time to diffuse from the ground to higher vertical levels, where it then was transported with higher wind speeds. Due to its location close to the ground and in a rather narrow valley, the wind speed at the upwind site was always significantly lower than at Mt. Schmücke ($< 1\,\mathrm{m\,s^{-1}}$ during both TE1 and 3). The SF_6 travelling times observed during the tracer experiments can thus be expected to be somewhat longer than the travelling times of “representative” air parcels during FCEs, which do not arise from a point source on the ground but rather travel with the higher wind speeds above the ground.

Results for TE2 and TE4 are given in Figs. S1 and S2 in the ESM. They show that during TE2 much lower mixing ratios than during TE1 and 3 were observed at the Mt. Schmücke (20) and the downwind sites (30 and 32), indicating that the SF_6 plume did indeed not directly pass these sites or that the vertical lifting from the upwind site was blocked. During TE4, mixing ratios even at the sites closest to the upwind site

ACPD
14, 1861–1917, 2014

(21 and 22) started only 40 min after the initial SF_6 release, indicating a strong decoupling/blocking of the upwind site. This finding of a possible upwind site blocking is also confirmed by the flow connectivity analysis. All results show that flow connectivity between the sites was likely not given during TE2 and 4.

Overall, the SF_6 tracer experiments serve to evidence two crucial assumptions/prerequisites of the HCCT-2010 campaign: (i) Under appropriate meteorological conditions a Lagrangian-type approach of data analysis is valid and (ii) the flow validation scheme developed in this work is suitable for identifying such conditions.

3.5 Overall evaluation of the FCEs

Finally, a critical assessment of meteorological and flow conditions during the ground-based cloud passage campaign HCCT-2010 has been made to conclusively validate the selected FCEs regarding the required conditions for the Lagrangian-type experiment, particularly, flow connectivity and other meteorological conditions. Thus, the obtained results, including pros and cons of each selected FCE, are outlined in Table 5. Moreover, an overall conclusive statement is given in Table 5 for each respective FCE regarding the suitability of its meteorological and flow connectivity conditions.

In total, Table 5 qualitatively concludes that the meteorological and flow connectivity conditions during the 14 FCEs mostly relatively well conform to the HCCT-2010 experiment concept. Furthermore, Table 5 showed that all listed FCEs have many pros but also minor cons. Thus, no final ranking of the listed FCEs has been done. Due to the fact that the comprehensive critical evaluation revealed that some of the FCEs provide somewhat more suitable conditions than others, it is noted that the disadvantages some FCEs needs to be kept mind during further investigations. Nevertheless, all FCEs and NCEs determined in the present study are recommended for further aimed investigations of the HCCT-2010 dataset.

ACPD
14, 1861–1917, 2014

4 Summary

The present study was aimed at the comprehensive evaluation of the required meteorological and connected flow conditions present during the ground-based Lagrangian-type experiment HCCT-2010 in order to provide evaluated suitable measurement time periods for further investigations. For this purpose, synoptic and local scale advection conditions during HCCT-2010 were examined and classified. The local flow conditions throughout the entire measurement period were studied by means of statistical analyses and corresponding statistical measures (COD and cross-correlation). For the statistical analyses, the measured concentrations of the quasi-inert trace gas ozone and selected particle number distribution bins measured at the upwind, summit and downwind site of the mountain ridge were used. The entire measurement period was analysed with respect to the prevalence of the same air mass at all sites and the presence or non-presence of a cloud at the different sites. By means of calculated statistical parameters and locally measured meteorological data, both FCEs and NCEs with suitable connected flow conditions were finally identified in a objective and automatic manner following a successive procedure based on predefined criteria. Additionally, the mesoscale airflow over the mountain ridge were characterised by means of the non-dimensional parameters, which were calculated from rawinsonde observation data. For the further verification of the local flow connectivity also tracer experiments with the inert gas SF_6 were conducted during the HCCT-2010 field campaign. The tracer experiment data were used for studies on local air transport processes in the experimental area. Moreover, the local meteorological conditions during the identified FCEs were studied in detail. An overall evaluation of meteorological and flow conditions of each identified FCEs provided finally the an assessment on each selected FCE.

The comprehensive examination showed that, especially for southwestern weather-type situations with stable incoming flow, orographic cloudiness was observed. In total, approx. one third of the examined HCCT-2010 cloud periods were characterised by orographic cloudiness and about two third by clouds occurring associated to syn-

ACPD
14, 1861–1917, 2014

optic fronts. The statistical flow analyses and tracer experiment data have shown that a strong link between the sites exists, particularly under constant south-westerly flow, high wind speed and slightly stable stratification conditions. The performed SF_6 tracer experiments have confirmed that under appropriate meteorological conditions a Lagrangian-type approach is valid and that the connected flow validation procedure developed in this work is suitable in identifying such required conditions. The overall evaluation resulted in 14 adequate FCEs, which mostly relatively well agree with the HCCT-2010 experiment concept and are hence useful for further studies.

Supplementary material related to this article is available online at http://www.atmos-chem-phys-discuss.net/14/1861/2014/acpd-14-1861-2014-supplement.zip.

Acknowledgements. This work was gratefully supported by the German Research Foundation (DFG, He 3086/15-1, DFG grant Me 3534/1-2).

References

Baines, P. G.: Topographic Effects in Stratified Flows, Cambridge University Press, Cambridge, 1995.

Boucher, O., Randall, D., Artaxo, P., Bretherton, C., Feingold, G., Forster, P., Kerminen, V.-M., Kondo, Y., Liao, H., Lohmann, U., Rasch, P., Satheesh, S. K., Sherwood, S., Stevens, B., and Zhang, X. Y.: Clouds and Aerosols, in: Climate Change 2013: The Physical Science Basis. Contribution of Working Group I to the Fifth Assessment Report of the Intergovernmental Panel on Climate Change, edited by: Stocker, T. F., Qin, D., Plattner, G.-K., Tignor, M., Allen, S. K., Boschung, J., Nauels, A., Xia, Y., Bex, V., and Midgley, P. M., Cambridge University Press, Cambridge, UK, New York, NY, USA, 1–139, in press, 2013.

Bower, B. K. N., Choularton, T. W., Gallagher, M. W., Beswick, K. M., Flynn, M. J., Allen, A. G., Davison, B. M., James, J. D., Robertson, L., Harrison, R. M., Hewitt, C. N., Cape, J. N.,

ACPD
14, 1861–1917, 2014

Critical assessment of meteorological conditions and airflow connectivity

A. Tilgner et al.

McFadyen, G. G., Milford, C., Sutton, M. A., Martinsson, B. G., Frank, G., Swietlicki, E., Zhou, J., Berg, O. H., Mentes, B., Papaspiropoulos, G., Hansson, H. C., Leck, C., Kulmala, M., Aalto, P., Vakeva, M., Berner, A., Bizjak, M., Fuzzi, S., Laj, P., Facchini, M. C., Orsi, G., Ricci, L., Nielsen, M., Allan, B. J., Coe, H., McFiggans, G., Plane, J. M. C., Collett, J. L., Moore, K. F., and Sherman, D. E.: ACE-2 HILLCLOUD, an overview of the ACE-2 ground-based cloud experiment, Tellus B, 52, 750–778, 2000.

Bower, K. N., Choularton, T. W., Gallagher, M. W., Colvile, R. N., Beswick, K. M., Inglis, D. W. F., Bradbury, C., Martinsson, B. G., Swietlicki, E., Berg, O. H., Cederfelt, S. I., Frank, G., Zhou, J., Cape, J. N., Sutton, M. A., McFadyen, G. G., Milford, C., Birmili, W., Yuskiewicz, B. A., Wiedensohler, A., Stratmann, F., Wendisch, M., Berner, A., Ctyroky, P., Galambos, Z., Mesfin, S. H., Dusek, U., Dore, C. J., Lee, D. S., Pepler, S. A., Bizjak, M., and Divjak, B.: The Great Dun Fell Experiment 1995: an overview, Atmos. Res., 50, 151–184, 1999.

Bruintjes, R. T., Clark, T. L., and Hall, W. D.: The dispersion of tracer plumes in mountainous regions in Central Arizona – comparisons between observations and modeling results, J. Appl. Meteorol., 34, 971–988, 1995.

Choularton, T. W., Colvile, R. N., Bower, K. N., Gallagher, M. W., Wells, M., Beswick, K. M., Arends, B. G., Mols, J. J., Kos, G. P. A., Fuzzi, S., Lind, J. A., Orsi, G., Facchini, M. C., Laj, P., Gieray, R., Wieser, P., Engelhardt, T., Berner, A., Kruisz, C., Moller, D., Acker, K., Wieprecht, W., Luttke, J., Levsen, K., Bizjak, M., Hansson, H. C., Cederfelt, S. I., Frank, G., Mentes, B., Martinsson, B., Orsini, D., Svenningsson, B., Swietlicki, E., Wiedensohler, A., Noone, K. J., Pahl, S., Winkler, P., Seyffer, E., Helas, G., Jaeschke, W., Georgii, H. W., Wobrock, W., Preiss, M., Maser, R., Schell, D., Dollard, G., Jones, B., Davies, T., Sedlak, D. L., David, M. M., Wendisch, M., Cape, J. N., Hargreaves, K. J., Sutton, M. A., StoretonWest, R. L., Fowler, D., Hallberg, A., Harrison, R. M., and Peak, J. D.: The Great Dun Fell Cloud Experiment 1993: an overview, Atmos. Environ., 31, 2393–2405, 1997.

Colle, B. A.: Sensitivity of orographic precipitation to changing ambient conditions and terrain geometries: an idealized modeling perspective, J. Atmos. Sci., 61, 588–606, 2004.

Colvile, R. N., Bower, K. N., Choularton, T. W., Gallagher, M. W., Wobrock, W., Hargreaves, K. J., Storeton-West, R. L., Cape, J. N., Jones, B., Wiedensohler, A., Hansson, H.-C., Wendisch, M., Acker, K., Wieprecht, W., Pahl, S., Winkler, P., Berner, A., and Kruisz, C.: Meteorology of the Great Dun Fell Cloud Experiment 1993, Atmos. Environ., 31, 2407–2420, 1997.

ACPD
14, 1861–1917, 2014

Critical assessment of meteorological conditions and airflow connectivity

A. Tilgner et al.

Draxler, R. and Rolph, G.: HYSPLIT (HYbrid Single-Particle Lagrangian Integrated Trajectory) Model access via NOAA ARL READY, NOAA Air Resources Laboratory, Silver Spring, MD, 2003.

Heinold, B., Tilgner, A., Jaeschke, W., Haunold, W., Knoth, O., Wolke, R., and Herrmann, H.: Meteorological characterisation of the FEBUKO hill cap cloud experiments – Part 2: Tracer experiments and flow characterisation with nested non-hydrostatic atmospheric models, Atmos. Environ., 39, 4195–4207, 2005.

Heintzenberg, J. and Charlson, R. J.: Clouds in the Perturbed Climate System: Their Relationship to Energy Balance, Atmospheric Dynamics, and Precipitation, MIT Press, Cambridge, MA, USA, 57 pp., 2009.

Herrmann, H., Wolke, R., Müller, K., Brüggemann, E., Gnauk, T., Barzaghi, P., Mertes, S., Lehmann, K., Massling, A., Birmili, W., Wiedensohler, A., Wieprecht, W., Acker, K., Jaeschke, W., Kramberger, H., Svrcina, B., Bächmann, K., Collett, J. L. J., Galgon, D., Schwirn, K., Nowak, A., Pinxteren, D. v., Plewka, A., Chemnitzer, R., Rüd, C., Hofmann, D., Tilgner, A., Diehl, K., Heinold, B., Hinneburg, D., Knoth, O., Sehili, A. M., Simmel, M., Wurzler, S., Majdik, Z., Mauersberger, G., and Müller, F.: FEBUKO and MODMEP: field measurements and modelling of aerosol and cloud multiphase processes, Atmos. Environ., 39, 4169–4183, 2005.

Jiang, Q. F.: Moist dynamics and orographic precipitation, Tellus A, 55, 301–316, 2003.

Krudysz, M. A., Froines, J. R., Fine, P. M., and Sioutas, C.: Intra-community spatial variation of size-fractionated PM mass, OC, EC, and trace elements in the Long Beach, CA area, Atmos. Environ., 42, 5374–5389, 2008.

Möller, D.: Chemistry of the Climate System, Walter de Gruyter, Berlin, 722 pp., 2010.

Ott, D. K., Kumar, N., and Peters, T. M.: Passive sampling to capture spatial variability in $PM_{10\text{-}2.5}$, Atmos. Environ., 42, 746–756, 2008.

Pinto, J. P., Lefohn, A. S., and Shadwick, D. S.: Spatial variability of $PM_{2.5}$ in urban areas in the United States, J. Air Waste Manage., 54, 440–449, 2004.

Pruppacher, H. R. and Jaenicke, R.: The processing of water-vapor and aerosols by atmospheric clouds, a global estimate, Atmos. Res., 38, 283–295, 1995.

Ravishankara, A. R.: Heterogeneous and multiphase chemistry in the troposphere, Science, 276, 1058–1065, 1997.

Rolph, G. D.: Real-time Environmental Applications and Display sYstem (READY) Website (http://ready.arl.noaa.gov), NOAA Air Resources Laboratory, Silver Spring, MD, 2013.

ACPD
14, 1861–1917, 2014

Critical assessment of meteorological conditions and airflow connectivity

A. Tilgner et al.

Sander, R.: Compilation of Henry's Law Constants for Inorganic and Organic Species of Potential Importance in Environmental Chemistry (Version 3), available at: http://www.henrys-law.org (last access: 15 July 2013), 1999.
Strunk, M., Engel, A., Schmidt, U., Volk, C. M., Wetter, T., Levin, I., and Glatzel-Mattheier, H.: CO_2 and SF_6 as stratospheric age tracers: consistency and the effect of mesospheric SF_6-loss, Geophys. Res. Lett., 27, 341–344, 2000.
Tilgner, A., Heinold, B., Nowak, A., and Herrmann, H.: Meteorological characterisation of the FEBUKO hill cap cloud experiments – Part 1: Synoptic characterisation of measurement periods, Atmos. Environ., 39, 4185–4194, 2005.
USEPA: Air Quality Criteria for Particulate Matter, National Center for Environmental Assessment, Office of Research and Development, US Environmental Protection Agency, Research Triangle Park, NC 27711, Washington, DC, Report No. EPA/600/P-99/002aF and EPA/600/P-99/002bF, 2004.
van Pinxteren, D., Brüggemann, E., Gnauk, T., Müller, K., Thiel, C., and Herrmann, H.: A GIS based approach to back trajectory analysis for the source apportionment of aerosol constituents and its first application, J. Atmos. Chem., 67, 1–28, doi:10.1007/s10874-011-9199-9, 2010.
Vosper, S. B., Mobbs, S. D., and Gardiner, B. A.: Measurements of the near-surface flow over a hill, Q. J. Roy. Meteor. Soc., 128, 2257–2280, 2002.
Wang, Y. G., Hopke, P. K., and Utell, M. J.: Urban-scale spatial-temporal variability of black carbon and winter residential wood combustion particles, Aerosol Air Qual. Res., 11, 473–481, 2011.
Wobrock, W., Schell, D., Maser, R., Jaeschke, W., Georgii, H. W., Wieprecht, W., Arends, B. G., Mols, J. J., Kos, G. P. A., Fuzzi, S., Facchini, M. C., Orsi, G., Berner, A., Solly, I., Kruisz, C., Svenningsson, I. B., Wiedensohler, A., Hansson, H. C., Ogren, J. A., Noone, K. J., Hallberg, A., Pahle, S., Schneider, T., Winkler, P., Winiwarter, W., Colcile, R., Choularton, T. W., Flossmann, A. I., and Borrman, S.: The Kleiner Feldberg cloud experiment 1990: an overview, J. Atmos. Chem., 19, 3–35, 1994.
Wongphatarakul, V., Friedlander, S. K., and Pinto, J. P.: A comparative study of $PM_{2.5}$ ambient aerosol chemical databases, Environ. Sci. Technol., 32, 3926–3934, 1998.

ACPD
14, 1861–1917, 2014

Table 1. Dates and times (CEST) and average meteorological conditions at Schmücke site for SF_6 tracer experiments.

	TE1	TE2	TE3	TE4
Date	20 Sep 2010	23 Sep 2010	6 Oct 2010	23 Oct 2010
SF_6 Release time	11:45–11:55	12:50–13:00	13:30–13:50	10:00–10:20
Sampling time	11:45–12:45	12:50–13:45	13:30–14:30	10:00–11:00
Meteorological conditions at Mt. Schmücke				
Temperature (°C)	7.5	14.5	10.3	−1.8
Relative humidity (RH, %)	76	68	99	94
Pressure (hPa)	907	905	905	901
Wind speed ($m\,s^{-1}$)	7.8	6.5	3.8	9.0
Wind direction (°)	240	218	220	223
Global radiation ($W\,m^{-2}$)	251	548	194	280
Cloud present at Schmücke?	No	No	Yes	Yes
Connected flow parameters				
COD_{O3} GL-SM	0.13	0.07	0.12	0.29
SM-GB	0.03	0.07	0.04	0.12
GL-GB	0.12	0.02	0.11	0.39
COD_{N49nm}GL-SM	0.03	0.30	0.08	0.25
SM-GB	0.08	0.06	0.05	0.11
GL-GB	0.08	0.33	0.08	0.31
COD_{N217nm}GL-SM	0.03	0.06	0.45	0.20
SM-GB	0.03	0.04	0.37	0.18
GL-GB	0.02	0.06	0.10	0.31

ACPD
14, 1861–1917, 2014

Table 2. Classification of the general weather situations and the associated air masses during the HCCT2010 field campaign and the offline-measurement periods with both online and offline sampling.

Date	General weather situation [a]	Predominant air mass [b]	Offline-measurement periods (CEST)
14 Sep	Trough Central Europe (TrM)	Marine air from North Atlantic (mPt)	14 Sep 2010 11:00 – 15 Sep 2010 02:00
15–17 Sep	Cyclonic West (WZ)	Greenlandic polar air (mP)	
18–23 Sep	Bridge over Central Europe (BM)	Warmed polar air (mPt)	
24 Sep	Transition (Ü)	Greenlandic polar air (mP)	24 Sep 2010 23:45 – 25 Sep 2010 01:45
25–28 Sep	Trough Central Europe (TM)	Greenlandic polar air (mP)	
29 Sep–3 Oct	High over Fennoscandia, cyclonic (HFZ)	Continental tropical air (cTp)	1 Oct 2010 22:30 – 2 Oct 2010 05:30; 2 Oct 2010 14:30 – 2 Oct 2010 20:00
4–9 Oct	Anticyclonic South (SA)	Mediterranean tropical air (mTs)	6 Oct 2010 12:15 – 7 Oct 2010 03:15
10–14 Oct	High over Norwegian Sea and Iceland, anticyclonic (HNA)	Continental polar air (cP)	
15 Oct	Transition (Ü)	Continental air Central Europe (cPt)	
16–21 Oct	Trough Central Europe (TrM)	Greenlandic polar air (mP)	19 Oct 2010 21:30 – 20 Oct 2010 03:30
22–24 Oct	Cyclonic West (WZ)	Arctic polar air (mPa)	24 Oct 2010 01:30 – 24 Oct 2010 08:45; 24 Oct 2010 09:15 – 24 Oct 2010 11:45

[a] Subjective Hess–Brezowsky classification (Hess and Brezowsky, 1952; revised by Gerstengarbe et al., 1999);
[b] European air-mass classification after Scherhag (1948).

ACPD
14, 1861–1917, 2014

Table 3. Overview of the statistical analysis of the connected flow and cloud conditions. Mean COD values, LWC, wind direction and speed at Mt. Schmücke (dd, ff), precipitation (RR) are presented for the selected FCEs.

FCE (time (CEST))	LWC $g\,m^{-3}$	dd SM °	ff SM $m\,s^{-1}$	COD SM-GL O_3	COD GB-SM O_3	COD GB-GL O_3	COD SM-GL N49nm	COD GB-SM N49nm	COD GB-GL N49nm	COD SM-GL N217 nm	COD GB-SM N217 nm	COD GB-GL N217 nm	RR SM mm
FCE1.1 (14 Sep 2010 11:00–15 Sep 2010 01:50)	0.25	236	8.2	0.06	0.04	0.03	0.06	0.08	0.03	0.74	0.75	0.14	1.2
FCE1.2 (15 Sep 2010 03:00–15 Sep 2010 06:20)	0.20	231	9.6	0.04	0.05	0.03	0.04	0.04	0.02	0.86	0.88	0.13	0.4
FCE2.1 (15 Sep 2010 23:00–16 Sep 2010 02:00)	0.17	240	8.7	0.02	0.02	0.02	0.03	0.08	0.09	0.71	0.72	0.09	0.0
FCE4.1 (16 Sep 2010 13:10–16 Sep 2010 15:00)	0.13	243	7.4	0.06	0.03	0.04	0.09	0.10	0.17	0.57	0.51	0.14	0.8
FCE5.1 (16 Sep 2010 21:40–16 Sep 2010 23:50)	0.30	239	6.3	0.05	0.03	0.03	0.04	0.10	0.12	0.89	0.87	0.13	0.0
FCE7.1 (24 Sep 2010 21:10–25 Sep 2010 00:50)	0.20	228	6.7	0.04	0.04	0.03	0.05	0.09	0.12	0.69	0.67	0.07	0.0
FCE11.2 (1 Oct 2010 20:50–2 Oct 2010 03:10)	0.37	222	3.7	0.08	0.10	0.14	0.09	0.06	0.12	0.59	0.51	0.15	0.0
FCE11.3 (2 Oct 2010 07:10–3 Oct 2010 00:30)	0.32	220	6.3	0.12	0.09	0.06	0.13	0.08	0.14	0.76	0.69	0.17	0.5
FCE13.3 (6 Oct 2010 06:50–7 Oct 2010 01:00)	0.32	223	4.2	0.10	0.06	0.07	0.11	0.09	0.15	0.50	0.41	0.12	0.0
FCE22.0 (19 Oct 2010 01:50–19 Oct 2010 09:00)	0.29	233	5.1	0.07	0.05	0.03	0.18	0.09	0.12	0.88	0.85	0.12	0.0
FCE22.1 (19 Oct 2010 21:10–20 Oct 2010 02:30)	0.31	248	4.7	0.07	0.05	0.09	0.09	0.04	0.09	0.83	0.78	0.13	0.2
FCE24.0 (21 Oct 2010 22:10–22 Oct 2010 10:00)	0.14	241	4.9	0.09	0.03	0.08	0.15	0.09	0.07	0.78	0.76	0.06	0.0
FCE26.1 (23 Oct 2010 23:40–24 Oct 2010 07:20)	0.19	233	9.7	0.03	0.04	0.01	0.10	0.04	0.09	0.86	0.84	0.08	0.8
FCE26.2 (24 Oct 2010 08:40–24 Oct 2010 12:20)	0.15	239	9.0	0.03	0.03	0.01	0.19	0.08	0.23	0.84	0.83	0.07	0.4

ACPD
14, 1861–1917, 2014

Table 4. List of the calculated Froude numbers (Fr) and Richardson numbers (Ri) as well as the used input data of the rawinsonde observations (from the German Weather Service station Meiningen) during or near the selected FCEs/NCEs.

Date/time (CEST)	U/dd (m s^{-1})	dΘ/dz (K m^{-1})	dU/dz (s^{-1})	N^2 (s^{-1})	Fr	Ri	Overflow y: yes, n: no	Stability	Ozon COD	N_{49nm} COD
14 Sep, 14:00	8/240	0.0054	0.0107	0.0002	0.85	1.62	y (decelerated)	stable	0.02	0.05
15 Sep, 02:00	6/225	0.0024	0.014	0.0001	0.68	0.42	y	stable	0.03	0.02
15 Sep, 14:00	6/235	−0.0033	0.0186	−0.0001	0	−0.32	y*	labile	0.02	0.07
16 Sep, 02:00	5/240	0.0034	0.0159	0.0001	1.13	0.46	y (decelerated)	stable	0.02	0.09
16 Sep, 14:00	6/250	−0.0011	0.0112	0	→ 0.00	−0.30	y*	labile	0.04	0.17
17 Sep, 02:00	6/270	0.0049	0.0147	0.0002	1.1	0.77	y (decelerated)	stable	0.03	0.08
19 Sep, 14:00	6/250	−0.0031	0.0086	−0.0001	→ 0.00	−1.40	y*	labile	0.04	0.07
20 Sep, 14:00	6/235	0.0028	0.0106	0.0001	0.73	0.83	y	stable	0.01	0.03
22 Sep, 14:00	3/220	−0.0017	0.0024	−0.0001	→ 0.00	−9.31	y*	labile	0.03	0.16
24 Sep, 02:00	8/220	0.0147	0.0209	0.0005	1.27	1.14	y (decelerated)	stable	0.06	0.05
24 Sep, 14:00	–/210	–	–	–	–	–	–	–	0.03	0.13
25 Sep, 02:00	4/270	0.0032	0.0049	0.0001	1.39	4.49	y (decelerated)	stable	0.10	0.15
27 Sep, 02:00	5/270	0.0041	0.0121	0.0001	1.12	0.97	y (decelerated)	stable	0.12	0.11
27 Sep, 14:00	3/260	0.0004	0.0075	0	0.55	0.22	y	stable	0.12	0.16
28 Sep, 14:00	6/230	0.0021	0.0022	0.0001	0.73	15.22	y	stable	0.28	0.18
1 Oct, 14:00	3/340	0.0067	0.0008	0.0002	2.2	326.54	n (stagnant area)	stable	0.07	0.29
2 Oct, 02:00	3/225	0.0064	0.0063	0.0002	2.33	5.6	n (stagnant area)	stable	0.13	0.08
2 Oct, 14:00	6/220	0.0034	0.0118	0.0001	0.81	0.82	y (decelerated)	stable	0.06	0.18
3 Oct, 02:00	6/220	0.0068	0.0057	0.0002	1.31	7.19	y (decelerated)	stable	0.29	0.10
3 Oct, 14:00	7/195	0.0023	0.009	0.0001	0.58	0.97	y	stable	0.03	0.20
5 Oct, 14:00	6/240	0.0063	0.0112	0.0002	1.2	1.72	y (decelerated)	stable	0.18	0.25
6 Oct, 02:00	5/220	0.0112	0.0174	0.0004	1.75	1.26	y (stagnant flow)	stable	0.17	0.06
6 Oct, 14:00	5/225	0.0027	0.0053	0.0001	0.85	3.23	y (decelerated)	stable	0.09	0.13
7 Oct, 02:00	5/240	0.0036	0.0085	0.0001	1.16	1.68	y (decelerated)	stable	0.14	0.27
7 Oct, 14:00	2/55	0.0024	0.0029	0.0001	2.43	10.03	n (stagnant area)	stable	0.05	0.21
8 Oct, 14:00	4/60	−0.0015	0.0019	−0.0001	→ 0.00	−13.79	y*	labile	0.11	0.08
9 Oct, 14:00	6/80	0.0032	0.0151	0.0001	0.85	0.48	y (decelerated)	stable	0.13	0.14
10 Oct, 02:00	7/85	0.0151	0.0219	0.0005	1.66	1.09	y (stagnant flow)	stable	0.09	0.09
11 Oct, 02:00	7/85	0.0187	0.0182	0.0006	1.78	1.95	y (stagnant flow)	stable	0.09	0.11
11 Oct, 14:00	6/70	0.0021	0.0155	0.0001	0.73	0.3	y	stable	0.09	0.04
12 Oct, 02:00	4/45	0.0175	0.0064	0.0006	3.32	14.76	n (stagnant area)	stable	0.11	0.06
13 Oct, 14:00	4/65	0.007	0.009	0.0002	1.83	2.97	y (stagnant flow)	stable	0.31	0.15
16 Oct, 02:00	4/245	0.0037	0.0087	0.0001	1.51	1.67	y (stagnant flow)	stable	0.12	0.20
19 Oct, 02:00	6/230	0.0062	0.0118	0.0002	1.12	1.57	y (decelerated)	stable	0.05	0.10
19 Oct, 14:00	7/230	0.002	0.0121	0.0001	0.6	0.47	y	stable	0.02	0.06
20 Oct, 02:00	6/245	0.0063	0.0185	0.0002	1.16	0.64	y (decelerated)	stable	0.06	0.07
21 Oct, 14:00	7/250	−0.0011	0.0069	0	→ 0.00	−0.79	y*	labile	0.03	0.11
22 Oct, 02:00	7/240	0.0101	0.0138	0.0004	1.23	1.88	y (decelerated)	stable	0.12	0.04
23 Oct, 14:00	8/225	0.0128	0.02	0.0005	1.25	1.14	y (decelerated)	stable	0.09	0.24
24 Oct, 02:00	13/225	0.0038	0.0286	0.0001	0.42	0.16	y	stable	0.01	0.08
24 Oct, 14:00	7/245	0	0.0073	0	0	0	y	neutral	0.02	0.19

ACPD
14, 1861–1917, 2014

ACPD
14, 1861–1917, 2014

Critical assessment of meteorological conditions and airflow connectivity

A. Tilgner et al.

Table 5. Summary of the meteorological and overflow conditions during the selected FCEs and conclusive assessment.

FCE Date/Time (CEST) (Offline sampling)	Remarks on meteorological conditions and flow connectivity
FCE1.1 14 Sep 2010 11:00 – 15 Sep 2010 01:50 (14 Sep 2010 11:00 – 15 Sep 2010 02:00)	Mostly good overflow conditions characterised by low COD_{O3} values (mean COD_{O3} < 0.06 at all sites) and COD_{N49nm} (mean $COD_{N49nm,GL\text{-}GB}$ < 0.08), CODs and cross-correlation analysis showed less sufficient flow conditions around 17:30–19:00 and particularly after midnight (correlations with the upwind site significantly lower indicating that slight luv blocking effects possible), stable SW flow conditions (dd_{SM} = 236°), moderate wind speed (ff_{SM} = 8.2 m s^{-1}), occurred precipitation at the beginning and end (total RR_{SM} ≈ 1.2 mm), longest FCE (15 h), cold front at the end, frontal cloudiness, stable thermal stratification, quite stable trajectories and air mass advection **→Suitable FCE with adequate meteorological / connected flow conditions**
FCE1.2 15 Sep 2010 03:00– 06:20 (–)	Good overflow conditions characterised by low COD_{O3} values (mean COD_{O3} < 0.05 at all sites) and COD_{N49nm} (mean $COD_{N49nm,GL\text{-}GB}$ ≈ 0.02), very congruent O_3 concentrations, cross-correlations analysis show reasonable r_{xcor} values ($r_{xcor,GB\text{-}GL}$ ≈ 0.7), stable SW flow conditions (dd_{SM} = 231°), high wind speed (ff_{SM} = 9.6 m s^{-1}), probably stable thermal stratification, slight precipitation at all sites (RR_{SM} ≈ 0.4 mm), increasing LWC from 0.05 to 0.28 g m^{-3}, unsteady cloud base height, quite short event (3 1/3 h) **→Suitable FCE, but short event, with adequate meteorological/ connected flow conditions**
FCE2.1 15 Sep 2010 23:00 – 16 Sep 2010 02:00 (–)	Stable SW wind conditions (dd_{SM} ≈ 240°), good flow connectivity, low COD_{O3} (permanently below 0.02) and COD_{N49nm} (mean $COD_{N49nm,GL\text{-}GB}$ ≈ 0.09), very congruent O_3 concentrations, high cross-correlations (0.6 < r_{xcor} < 0.8), stable thermal stratification, slightly decelerated flow possible (Fr = 1.13), moderate to high wind speed (ff_{SM} increasing from about 7 m s^{-1} to 10.5 m s^{-1}), increasing cloud base height at the end (> 300 m), relatively low LWC (mean 0.17 g m^{-3}), short duration (3 h), no precipitation, clouds probably not purely orographically induced **→Suitable FCE with adequate meteorological/ connected flow conditions**
FCE4.1 16 Sep 2010 13:10–15:00 (–)	Less sufficient overflow conditions, COD_{O3} (mean COD_{O3} < 0.07 at all sites), high COD_{N49nm} (mean $COD_{N49nm,GL\text{-}GB}$ ≈ 0.17), similar O_3 concentrations but low cross-correlations especially for the downwind site (slight disconnection possible), unstable wind direction changing from SW (224°) to WSW (254°) within 2 h, moderate wind speeds (ff_{SM} = 7.4 m s^{-1}), changing cloud base height (partly above 350 m at the end), labile thermal stratification (possible entrainment), low mean LWC (0.13 g m^{-3}), slight precipitation at all sites during the event (RR_{SM} < 0.8 mm) due to an occlusion (frontal cloudiness), only 2 h duration **→Probably useful FCE, with slightly limited meteorological and connected flow conditions**
FCE5.1 16 Sep 2010 21:40–23:50 (–)	Stable WSW flow conditions (dd_{SM} = 239°), reasonable connected flow conditions, COD_{O3} (mean COD_{O3} < 0.05 at all sites), COD_{N49nm} (mean $COD_{N49nm,GL\text{-}GB}$ ≈ 0.12), lower $COD_{N49nm,GL-SM}$ (≈ 0.04), similar O_3 concentrations profiles, moderate wind speeds (ff_{SM} = 6.3 m s^{-1}), stable thermal stratification, slightly decelerated flow possible (Fr = 1.1), quite stable cloud base height (200–250 m), stable and high LWC (mean 0.3 g m^{-3}), no precipitation, short cloud event (2:10 h) **→Suitable FCE, but short event, with adequate meteorological/connected flow conditions**
FCE7.1 24 Sep 2010 21:10 – 25 Sep 2010 00:50 (24 Sep 2010 23:45 – 25 Sep 2010 01:45)	Good overflow conditions, low COD_{O3} values (mean COD_{O3} < 0.04 at all sites), moderate COD_{N49nm} values (mean $COD_{N49nm,GL\text{-}GB}$ < 0.12), congruent O_3 concentrations, very high cross-correlations (0.8 < r_{xcor} < 0.9), stable SW winds (dd_{SM} = 228°), moderate wind speeds (mean ff_{SM} = 6.7 m s^{-1}), orographic cloudiness, relatively stable cloud base height of about 200–250 m with an increasing LWC of about 0.1 to 0.3 g m^{-3}, orographic cloudiness, no precipitation, quite stable thermal stratification, slightly decelerated flow possible at the end (slight LUV blocking, Fr = 1.4 and increasing CODs), slightly changing trajectories and air mass advection, relatively short event (3:40 h), conditions during the offline sampling period not as adequate as before **→Suitable FCE with adequate meteorological/connected flow conditions**
FCE11.2 1 Oct 2010 20:50 – 2 Oct 2010 03:10 (1 Oct 2010 22:30 –2 Oct 2010 05:30)	Reasonable overflow conditions, relatively high COD_{O3} values (mean $COD_{O3,GL\text{-}GB}$ ≈ 0.14) and COD_{N49nm} values (mean $COD_{N49nm,GL\text{-}GB}$ ≈ 0.12), lower values just for $COD_{N49nm,SM\text{-}GB}$ ≈ 0.06), indicating a slight LUV blocking at the beginning, upwind site ozone concentration profiles partly dissimilar, cross-correlation analysis shows partly quite high values, stable SW flow conditions (dd_{SM} = 222°), weak winds (ff_{SM} = 3.7 m s^{-1}), overflow possible (slight blocking effects, Fr = 2.2), very stable stratification, frontal cloudiness (occlusion front), slightly fluctuating cloud base height (100–200 m), increasing high LWC (mean 0.37 g m^{-3}), no precipitation, slightly changing trajectory pattern (6:20 h duration), conditions at the end of the offline sampling even less adequate as during the FCE (cp. COD analysis data in the ESM) **→Probably useful FCE with adequate meteorological but restricted connected flow conditions**
FCE11.3 2 Oct 2010 07:10 – 3 Oct 2010 00:30 (2 Oct 2010 14:30–20:00)	Almost good mountain overflow conditions, partly high COD values (mean $COD_{O3,GL\text{-}GB}$ ≈ 0.06; mean $COD_{N49nm,GL\text{-}GB}$ ≈ 0.14), higher values mostly for the upwind site, Fr (0.8; 1.3) and Ri (0.8; 7.2) numbers indicating a stable stratification and the possibility of a slightly decelerated flow, higher cross-correlations during 1st half of the FCE compared to the 2nd half, stable SW flow conditions (dd_{SM} = 220°), moderate to high wind speeds (mean ff_{SM} = 6.3 m s^{-1}, 3.6–9.2 m s^{-1}), slight precipitation (RR_{SM} ≈ 0.5 mm) particularly in first half of the FCE, frontal cloudiness (associated with warm front), variable cloud height (100–300 m), partly high LWC values (mean 0.32 g m^{-3}), stable trajectory pattern, long FCE (17:20 h duration) **→Suitable FCE with adequate meteorological/ connected flow conditions**

Table 5. Continued.

FCE Date/Time (CEST) (Offline sampling)	Remarks on meteorological conditions and flow connectivity
FCE13.3 6 Oct 2010 06:50 – 7 Oct 2010 01:00 (06.10-2010 12:15 – 7 Oct 2010 03:15)	Reasonably good overflow conditions, partly high COD values (mean $COD_{O3,GL\text{-}GB} \approx 0.07$; mean $COD_{N49nm,GL\text{-}GB} \approx 0.15$), Fr (0.85; 1.2) and Ri (3.2; 1.7) numbers indicating a stable stratification and the possibility of a slightly decelerated flow, upwind site ozone concentration profiles partly dissimilar, higher cross-correlations during 1st half of the FCE compared to the 2nd half (overall $r_{xcor} > 0.8$), stable SW flow conditions ($dd_{SM} = 223°$) with weak wind speeds ($ff_{SM} = 4.2\,m\,s^{-1}$), orographic cloudiness, relative stable cloud base height (200 to 100 m), high LWC values (mean $0.32\,g\,m^{-3}$, $LWC_{max} = 0.58\,g\,m^{-3}$), no precipitation, unstable trajectories, long cloud event (15 h duration), flow conditions at the end of the offline sampling event inadequate (see COD analysis in the ESM) **→Suitable FCE with partly adequate meteorological/ connected flow conditions**
FCE22.0 19 Oct 2010 01:50 – 19 Oct 2010 09:00 (–)	Mostly good overflow conditions, relatively low COD_{O3} values (mean $COD_{O3,GL\text{-}GB} < 0.03$), COD_{N49nm} (mean $COD_{N49nm,GL\text{-}GB} < 0.12$), congruent O_3 concentrations, very high cross-correlations ($r_{xcor} > 0.9$), stable thermal stratification, slightly decelerated flow possible at the start only (Fr = 1.1), stable SW winds (mean $dd_{SM} = 233°$), moderate wind speeds (mean $ff_{SM} = 5.1\,m\,s^{-1}$), relatively stable cloud base height (200-100 m), moderate LWC values (0.2–0.4 $g\,m^{-3}$), temperature below zero, low clouds and slight precipitation at the end due to an occlusion **→Suitable FCE with adequate meteorological/ connected flow conditions**
FCE22.1 19 Oct 2010 21:10 – 20 Oct 2010 02:30 (19 Oct 2010 21:30 – 20 Oct 2010 03:30)	Good overflow conditions, reasonable COD_{O3} values (mean $COD_{O3,GL\text{-}GB} = 0.09$), COD_{N49nm} (mean $COD_{N49nm,GL\text{-}GB} = 0.09$), less congruent O_3 concentrations, reasonable cross-correlations, stable thermal stratification, slightly decelerated flow possible at the end (Fr = 1.2), WSW to W flow conditions (mean $dd_{SM} = 248°$), low/moderate wind speed (mean $ff_{SM} = 4.7\,m\,s^{-1}$), varying cloud height (100 to 200 m), almost constant LWC (mean $0.31\,g\,m^{-3}$), precipitation occurred ($RR_{SM} < 0.2$ mm), reasonably stable trajectories, long event (5:20 h duration), flow conditions during the end of the offline sampling event still adequate (see COD analysis in the ESM) but precipitation at all sites **→Suitable FCE with adequate meteorological/ connected flow conditions**
FCE24.0 21 Oct 2010 22:10 – 22 Oct 2010 10:00 (–)	Partly good overflow conditions, reasonable mean COD_{O3} ($COD_{O3,GL\text{-}GB} = 0.08$) and partly high COD_{N49nm} ($COD_{N49nm,GL-SM} = 0.15$), ozone concentrations partly incongruent during night, good cross-correlation between the summit and downwind site ($r_{xcor,SM\text{-}GB} \approx 0.7$), r_{xcor} for the upwind site lower (< 0.3), cross-correlation imply a slight LUV blocking at the start, stable thermal stratification, slightly decelerated flow possible (Fr = 1.2), stable WSW flow conditions (mean $dd_{SM} = 241°$), moderate wind speed (mean $ff_{SM} = 4.9\,m\,s^{-1}$), unsteady cloud base height (170–350 m), quite low LWC values (mean $0.14\,g\,m^{-3}$), no precipitation, temperature below zero, orographic cloudiness, stable trajectories, long event (11:50 h duration) **→Probably useful FCE with acceptable meteorological and partly restricted connected flow conditions**
FCE26.1 23 Oct 2010 23:45 – 24 Oct 2010 07:20 (24 Oct 2010 01:30–08:45)	Good overflow conditions, low COD_{O3} ($COD_{O3,GL\text{-}GB} = 0.01$) and COD_{N49nm} ($COD_{N49nm} < 0.1$), congruent ozone concentrations, high overall cross-correlations ($0.7 < r_{xcor} < 0.9$), low Fr number (Fr = 0.42), stable stratification, stable SW flow conditions (mean $dd_{SM} = 233°$), high wind speed (mean $ff_{SM} = 9.7\,m\,s^{-1}$), inconsistent trajectories, post-frontal clouds probably not pure orographic, relatively stable LWC (mean $0.19\,g\,m^{-3}$), variable cloud base height (300–130 m), light precipitation during the FCE ($RR_{SM} < 0.8$), 07:35 h duration, flow conditions during the end of the offline sampling event still adequate (see COD analysis in the ESM) but precipitation at all sites **→Suitable FCE with adequate meteorological/ connected flow conditions**
FCE26.2 24 Oct 2010 08:40–12:20 (24 Oct 2010 09:15–11:45)	Probably good overflow conditions, low COD_{O3} ($COD_{O3,GL\text{-}GB} = 0.01$) but rather high COD_{N49nm} ($COD_{N49nm,GL\text{-}GB} = 0.23$), congruent ozone concentrations, good cross-correlations ($0.65 < r_{xcor} < 0.85$), low Fr number, SW–WSW flow conditions (mean $dd_{SM} = 239°$), high wind speed (mean $ff_{SM} = 9.0\,m\,s^{-1}$), inconsistent trajectories, post-frontal cloudiness and precipitation ($RR_{SM} < 0.4$), cloud base height at about 200 m increasing above 350 m at the end, decreasing LWC (mean $0.15\,g\,m^{-3}$), 03:40 h duration **→Suitable FCE, but short event, with adequate meteorological and most likely adequate connected flow conditions**

ACPD
14, 1861–1917, 2014

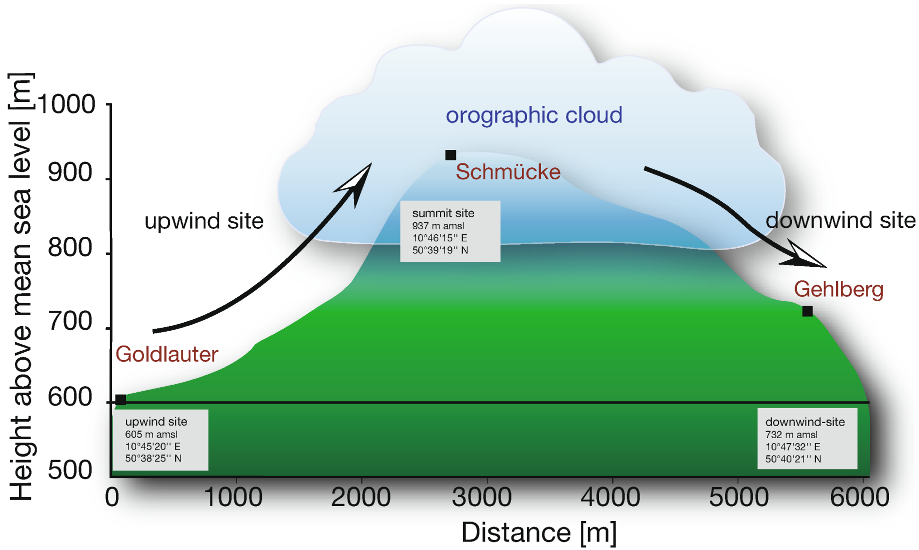

Fig. 1. Schematic depiction of the HCCT-2010 measurement area and the three sampling sites including the upwind site (Goldlauter), the summit/in-cloud site (Mt. Schmücke) and the downwind site (Gehlberg).

ACPD
14, 1861–1917, 2014

Critical assessment of meteorological conditions and airflow connectivity

A. Tilgner et al.

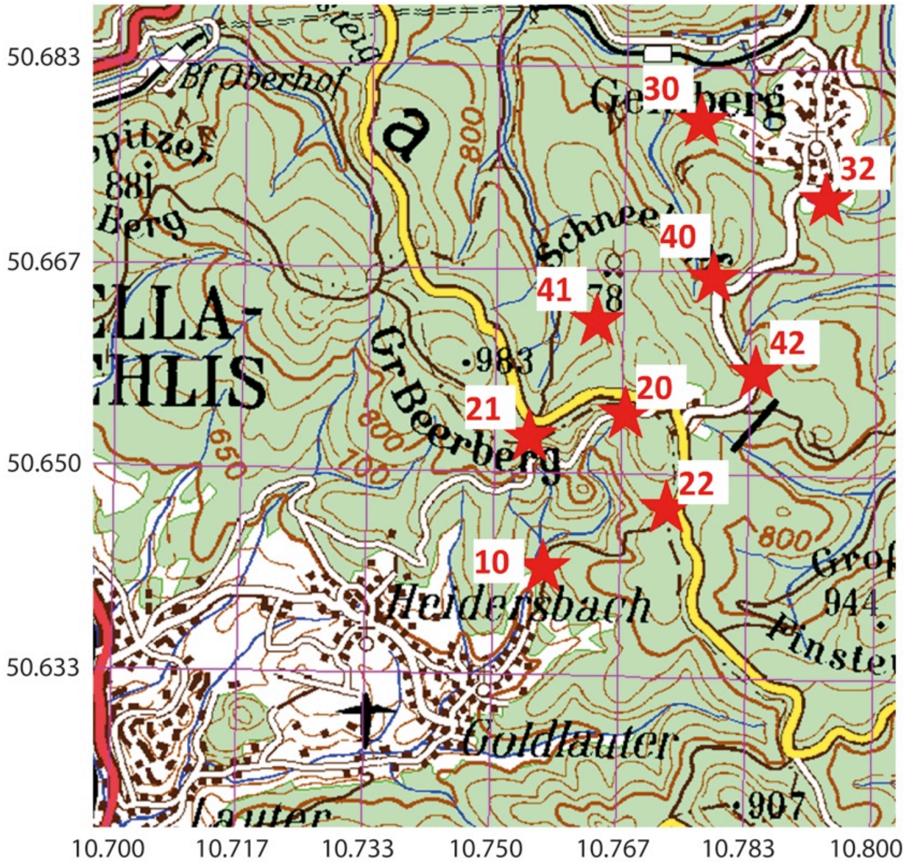

Fig. 2. Locations of all tracer experiment sampling sites, including the upwind release site Goldlauter (10), the summit site Mt. Schmücke (20) and the Gehlberg downwind site (32) (Map source: Thüringer Landesvermessungsamt).

ACPD
14, 1861–1917, 2014

Critical assessment of meteorological conditions and airflow connectivity

A. Tilgner et al.

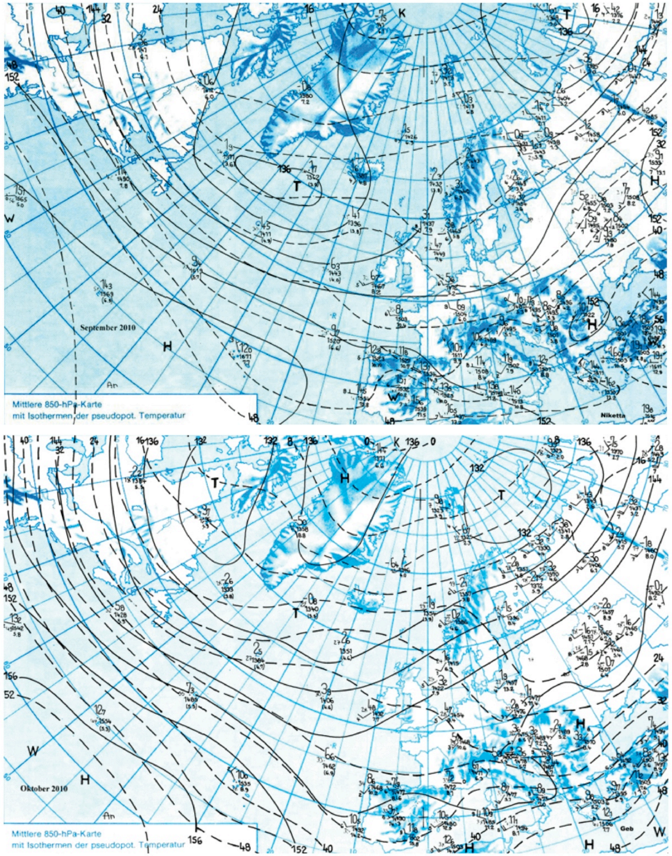

Fig. 3. Averaged synoptic situation (850 hPa level) over the North Atlantic and Europe in September 2010 and October 2010 including isotherms of the pseudo-potential temperature (source: Berliner Wetterkarte e.V., 2010).

ACPD
14, 1861–1917, 2014

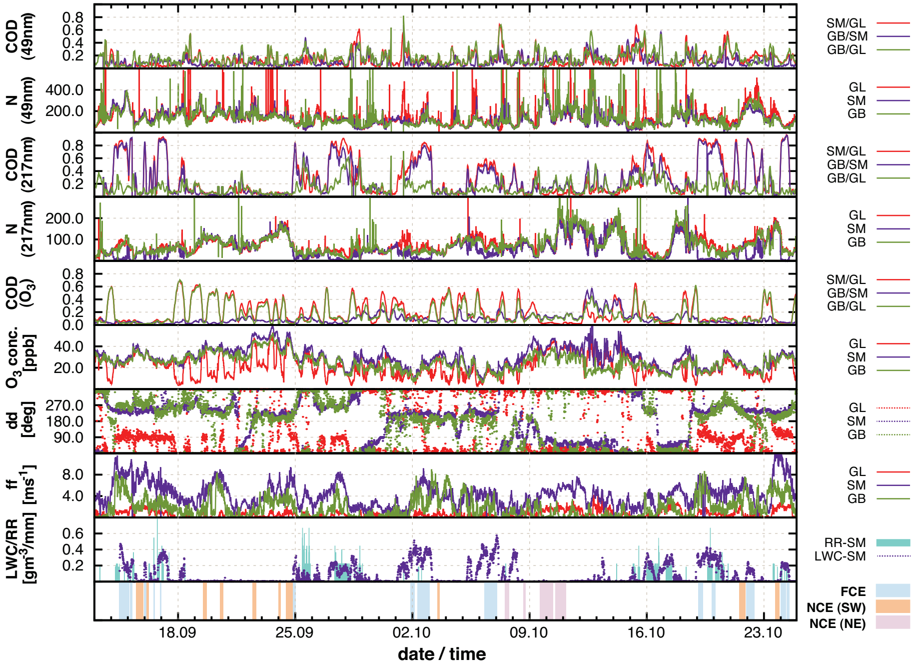

Fig. 4. Depiction of the measured meteorological parameters (wind direction (dd), wind speed (ff), precipitation (RR), cloud liquid water content (LWC)), ozone and particle concentrations (size bins N_{49nm} and N_{217nm}) and the calculated COD values.

ACPD
14, 1861–1917, 2014

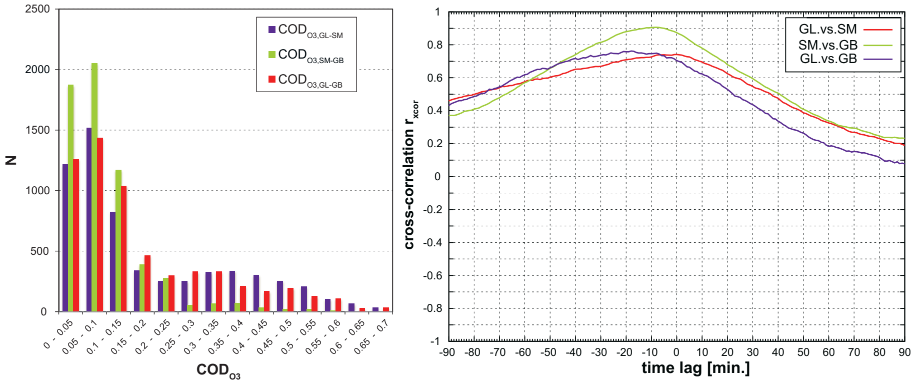

Fig. 5. Histogram of the calculated COD_{O3} values throughout the whole investigation period of HCCT-2010 (left) and calculated cross correlation (r_{xcor}) between the different sites (GL: upwind site; SM: summit site; GB: downwind site) based on measured ozone concentrations for a selected time period (right, 14 October 2010 11:00 CEST–15 October 2010 01:00 CEST).

ACPD
14, 1861–1917, 2014

Title Page
Abstract | Introduction
Conclusions | References
Tables | Figures
◀| |▶
◀ ▶
Back | Close
Full Screen / Esc
Printer-friendly Version
Interactive Discussion

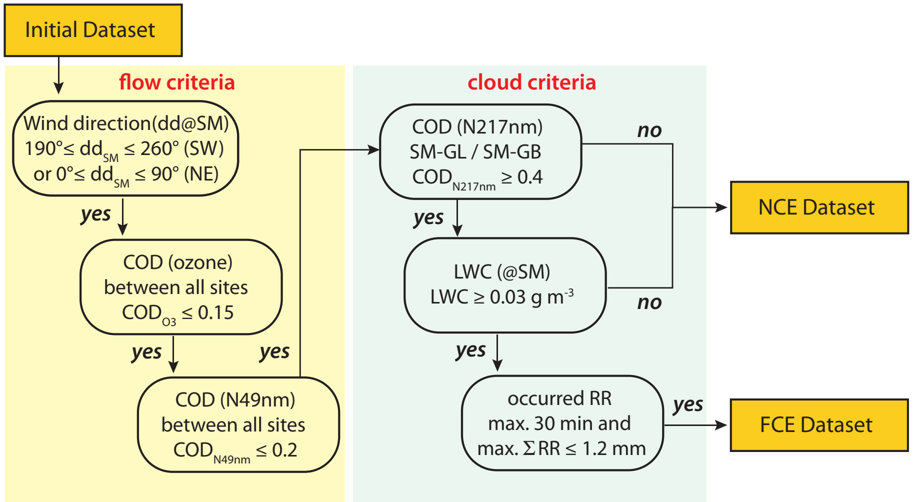

Fig. 6. Schematic depiction of the FCE and NCE selection procedure.

ACPD
14, 1861–1917, 2014

Critical assessment of meteorological conditions and airflow connectivity

A. Tilgner et al.

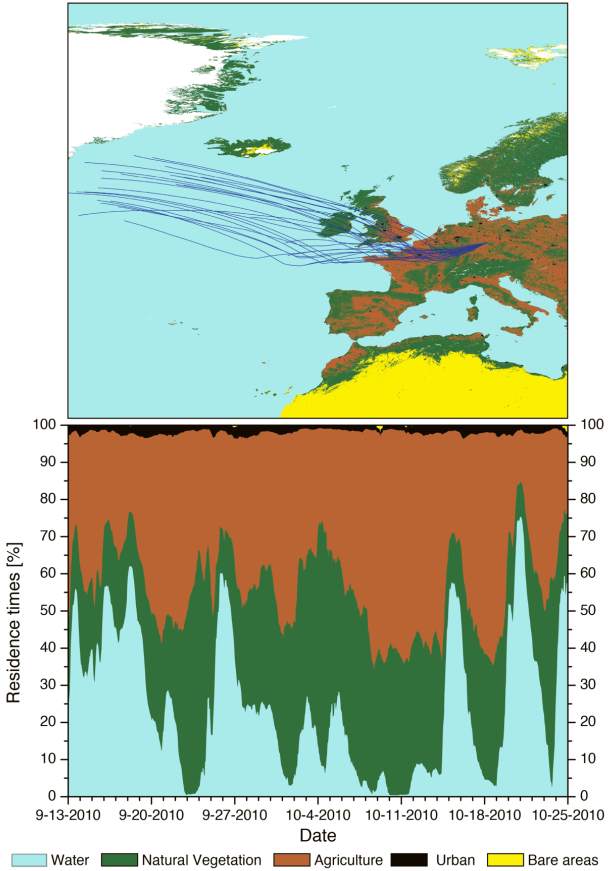

Fig. 7. Depiction of the calculated ensemble backward trajectories using the NOAA HYSPLIT model arriving at 14 September 2010 16:00 UTC at Mt. Schmücke (top) and the calculated residence times of all backward trajectories over different area categories throughout the HCCT-2010 campaign.

ACPD
14, 1861–1917, 2014

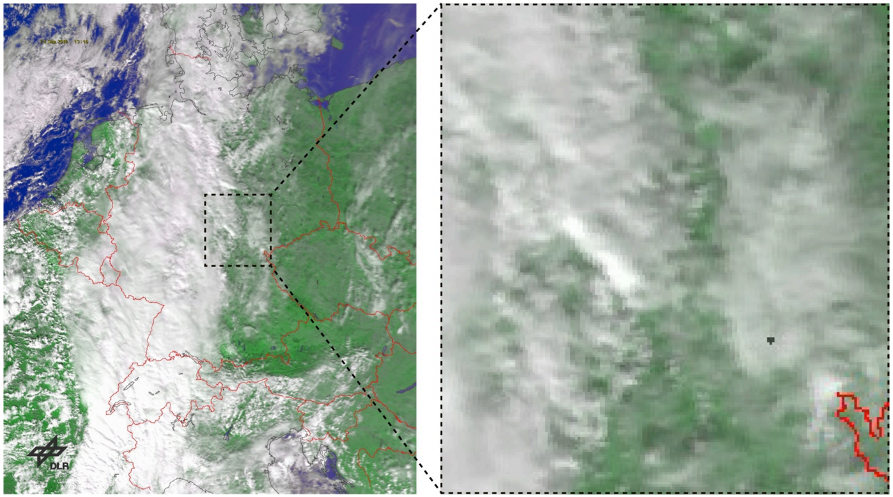

Fig. 8. Satellite picture demonstrating the orographic cloud at Mt. Schmücke (source: DLR).

ACPD
14, 1861–1917, 2014

Critical assessment of meteorological conditions and airflow connectivity

A. Tilgner et al.

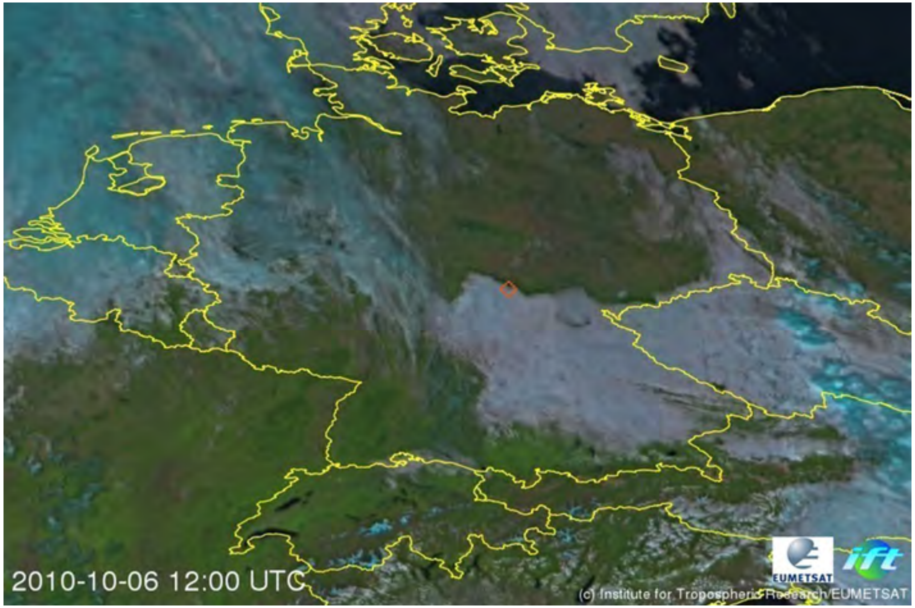

Fig. 9. Satellite picture of the cloud coverage over Germany (© TROPOS/EUMETSAT).

ACPD
14, 1861–1917, 2014

Critical assessment of meteorological conditions and airflow connectivity

A. Tilgner et al.

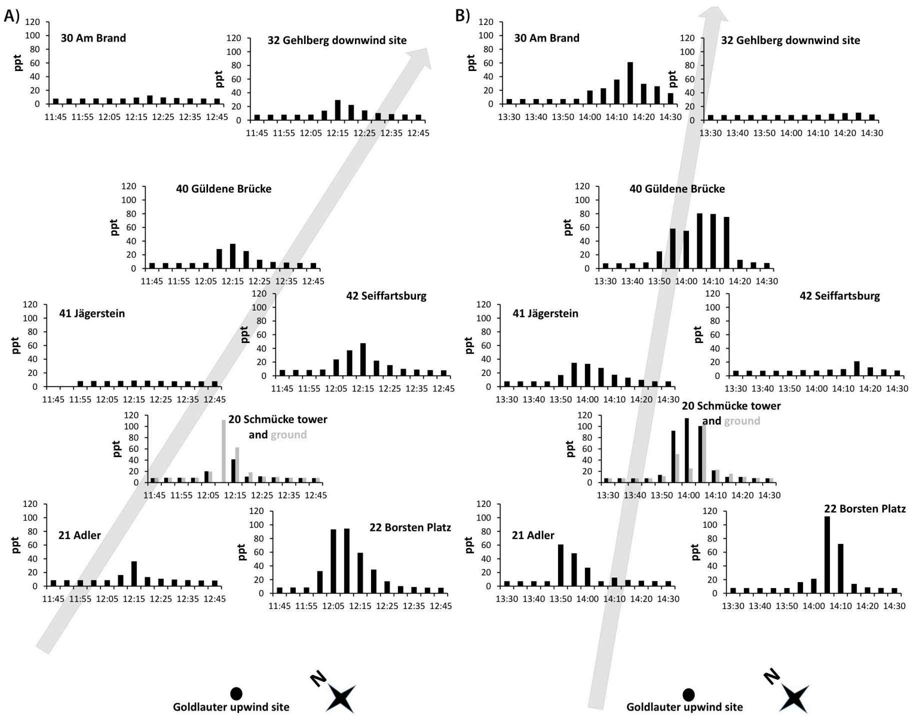

Fig. 10. SF_6 mixing ratios at different sites during **(A)** TE1 and **(B)** TE3. The bar plots indicate the approximate geographic position of the sites and the grey arrow indicates the mean wind direction at the Schmücke during the experiments. SF_6 release was at the Goldlauter upwind site.